

This is an Open Access document downloaded from ORCA, Cardiff University's institutional repository:<https://orca.cardiff.ac.uk/id/eprint/170414/>

This is the author's version of a work that was submitted to / accepted for publication.

Citation for final published version:

Sheng, Kangling, Wang, Xiaojun, Si, Fangyuan, Zhou, Yue, Liu, Zhao, Hua, Haochen, Wang, Xihao and Duan, Yuge 2024. Rational capacity investment for renewable hydrogen-based steelmaking systems: A multi-stage expansion planning strategy. *Applied Energy* 372, 123746. 10.1016/j.apenergy.2024.123746

Publishers page: <http://dx.doi.org/10.1016/j.apenergy.2024.123746>

Please note:

Changes made as a result of publishing processes such as copy-editing, formatting and page numbers may not be reflected in this version. For the definitive version of this publication, please refer to the published source. You are advised to consult the publisher's version if you wish to cite this paper.

This version is being made available in accordance with publisher policies. See <http://orca.cf.ac.uk/policies.html> for usage policies. Copyright and moral rights for publications made available in ORCA are retained by the copyright holders.



Highlights

Rational capacity investment for renewable hydrogen-based steelmaking systems: a multi-stage expansion planning strategy

Kangling Sheng, Xiaojun Wang, Fangyuan Si, Yue Zhou, Zhao Liu, Haochen Hua, Xihao Wang, Yuge Duan

- Rational capacity investments for RHSS from 2025 to 2050.
- Develop a multi-stage expansion planning model for RHSS.
- RHA can improve computational efficiency and achieve an optimal solution in a reasonable time frame.
- Sensitivity analysis shows the discount rate as the key factor in the planning results.
- The adaptability of RHA is evaluated through robustness analysis.

Rational capacity investment for renewable hydrogen-based steelmaking systems: a multi-stage expansion planning strategy

Kangling Sheng^a, Xiaojun Wang^a, Fangyuan Si^{a,*}, Yue Zhou^b, Zhao Liu^a, Haochen Hua^c, Xihao Wang^a, Yuge Duan^a

^a*School of Electrical Engineering, Beijing Jiaotong University, Beijing 100044, China*

^b*School of Engineering, Cardiff University, Cardiff CF24 3AA, UK*

^c*School of Energy and Electrical Engineering, Hohai University, Nanjing 211100, China*

Abstract

To improve energy efficiency and mitigate environmental impact, the iron and steel industry (ISI) is responsible for implementing a low-carbon transition. The renewable hydrogen-based steelmaking system (RHSS) has emerged as an innovative energy system in the pathway of reducing the carbon footprint of ISI. Nonetheless, the sustainable development requirements of RHSS emphasize the critical need for well-planned capacity investments to boost its economic viability. This study introduces a novel planning strategy for RHSS referred to as a multi-stage expansion planning (MSEP) model, which is aimed to minimize the levelized cost of crude steel over the planning horizon from 2025 to 2050 (EU climate neutrality year). The MSEP model incorporates the construction sequence and dynamic techno-economic parameters to formulate investment strategies that adapt to changing system requirements and external conditions over the planning horizon. To address the complexity of the MSEP model, a rolling-horizon approach (RHA) is proposed to solve the model sequentially while integrating updated information. The proposed approach is benchmarked against both the single-stage approach and the perfect-sight approach through case studies. The numerical results show that the proposed RHA (i) guarantees a rational capacity investment strategy for RHSS considering the construction sequence and dynamic techno-economic parameters over multiple planning stages; (ii) achieves a reduction in the levelized cost of crude steel by approximately 50% relative to the single-stage approach; (iii) resolves the convergence issues encountered with the perfect-sight approach while achieving an optimal solution in a reasonable time frame. Additionally, sensitivity analysis evaluates the uncertainties of multiple factors on the planning results, while the robustness analysis confirms the applicability and adaptability of RHA across various scenarios.

Keywords:

Multi-stage expansion planning, Rational capacity investment, Rolling-horizon approach, Renewable hydrogen-based steelmaking

1. Introduction

1.1. Background

Accelerating the low-carbon energy transition has become a global consensus [1]. In the face of escalating environmental and social pressures, the UN's global roadmap has announced ambitious commitments to achieve net-zero emissions by 2050 [2]. The iron and steel industry

*footnote: The short version of the paper was presented at ICAE2023, Doha, Qatar, Dec 3-5, 2023. This paper is a substantial extension of the short version of the conference paper.

Nomenclature
Sets

S	Set of typical seasonal days	ΔP^{el}	Ramp limitation of EL module [kW/h]
T	Set of timeslots (hours)	P^{el}	Electricity input of EL module [kW]
M	Set of equipment types	G^{el}	H ₂ output of EL module [kg _{H₂}]
N	Set of planning stages	$s^{\text{el}}/d^{\text{el}}$	Start-up/shut-down operation of EL module (integer)
Y	Set of planning years	u^{el}	On/off state of EL module (int.)
Z	Set of raw materials	$\bar{s}^{\text{el}}/\bar{d}^{\text{el}}$	Number of start-up/shut-down operations of the EL cluster (int.)

Indices

u	Index of foresight horizon	$S_{\text{max}}^{\text{el}}/D_{\text{max}}^{\text{el}}$	Num. of maximum start-ups/shut-downs operations of EL module per day (int.)
k	Index of the EL module	E^{ht}	State of charge of HT
d	Index of the number of years	$G^{\text{ht.c/d}}$	H ₂ charging/discharging [kg _{H₂}]
i	Index of planning stage	$\eta_{\text{max}}^{\text{ht}}$	Maximum charging/discharging ratio of HT
m	Index of equipment type	$\omega^{\text{ht.c/d}}$	Charging/discharging efficiency of HT
t	Index of time period (hour)	δ^{ht}	Self-discharge rate of HT
s	Index of typical day	K	Num. of planned EL modules (int.)

Parameters

c^{inv}	Capital expenditure for unit capacity configuration	I^{sf}	DRI output of SF [t_{DRI}]
c^{mai}	Operational expenditure rate	$\eta_{\text{min/max}}^{\text{sf}}$	Minimum/maximum operating ratio of SF
R	Discount factor	G^{sf}	H ₂ input of SF [kg _{H₂}]
λ	Technical life [year]	$\omega^{\text{sf.DRI/e}}$	Reduction/power consumption efficiency of SF
δ	Residual rate	P^{sf}	Electricity input of SF [kW]
r	Discount rate	S^{eaf}	Crude steel output of EAF [t_{CS}]

Variables

Q_z	Consumption of raw materials	S^{cs}	Crude steel load demand [t_{CS}]
c_z	Unit cost of raw materials z	$\eta_{\text{min/max}}^{\text{eaf}}$	Minimum/maximum operating ratio of EAF
ρ	Renewable energy penetration rate	$\omega^{\text{eaf.DRI/scrap}}$	Crude steel production ratio of DRI and scrap steel
ε	CO ₂ intensity [kg _{CO₂} / t_{cs}]	$\omega^{\text{eaf.e}}$	Electricity consumption efficiency of EAF
$P^{\text{wt/pv.N}}$	Normalized WT/PV generation [pu]	Q^{scrap}	Scrap steel input of EAF
$P^{\text{wt/pv}}$	Electricity output of WT/PV [kW]	P^{eaf}	Electricity input of EAF [kW]
		P^{grid}	Electricity purchased from power grid [kW]

6 (ISI), known for its high energy and CO₂ intensity, accounts for approximately 8% of the global
7 final energy demand and 7% of energy sector CO₂ emissions [3]. On average, the production of
8 one ton of steel requires 5.17 MWh of primary energy and releases 1.9 tonnes of CO₂ [4]. As
9 the world’s leading steel producer and consumer, China’s annual steel production exceeded one
10 billion tonnes in 2023, accounting for 54% of the global steel production [5]. The CO₂ emissions
11 from China’s steel production accounted for over 60% of global CO₂ emissions in this sector,
12 making it the largest single contributor to CO₂ emissions within the global steel industry [6].

13 Electrification of the industry can entirely abate the energy-related CO₂ emissions, reducing
14 the industry bottleneck to only residual process emissions [7]. An increasingly preferred strategy
15 for the electrification of ISI is the application of electric arc furnaces (EAF), which is especially
16 favored by its potential for flexibility [8], low environmental impact [9], and scrap steel recycling
17 [10]. Almost 20% of steel production worldwide and over 40% in the EU uses EAF to process
18 recycled scrap steel [11]. However, as electricity is one of the dominant contributors of inputting
19 energy in EAF, with the consumption of about 320-580 kWh/*t_{cs}* in general [12], the economic
20 feasibility of EAF is heavily dependent on the level of electricity consumption and the electricity
21 price.

22 As the energy system is transitioning towards a higher share of renewable energy resources
23 (RES) [13], RES is expected to grow with the active and broad implementation in the electri-
24 fication of ISI. The rapid decline in costs associated with the proliferation of renewable energy
25 technologies [14], forthcoming options to increase the uptake of RES as one possible way to
26 reduce energy consumption and CO₂ emissions in the electrification of ISI. Green hydrogen
27 produced by water electrolysis using RES offers the necessary flexibility to tackle with the
28 variability of RES [15]. In addition to serving as a clean energy source, hydrogen also plays a
29 critical role as a reducing agent in the iron ore reduction process [16]. In contrast to traditional
30 carbon-intensive steelmaking routes, such as blast furnace basic oxygen furnace (BF-BOF) and
31 natural gas-based direct reduction ironing followed by electric arc furnace (NG-DRI-EAF), the
32 hydrogen-based direct iron ore reduction followed by electric arc furnace (HDRI-EAF) route is
33 emerging as a promising alternative, which uses hydrogen instead of carbon-based reductants
34 such as coke and natural gas, exemplifies a significant shift from carbon-based to hydrogen-
35 based steelmaking pathways [17].

36 In recent years, several projects have been launched worldwide to explore the technical and
37 commercial viability of the HDRI-EAF route, including the EU-funded H2FUTURE project
38 [18], the SALCOS project in Germany [19], the POSCO project in South Korea [20], and
39 the Baowu project in China [21]. The MIDREX and HYL III processes, as the primary gas-
40 based direct reduction method for producing DRI, accounting for approximately 80% of the
41 global steel production based on shaft furnaces (SF) [22]. In addition, the possibility of flexible
42 use of up to 100% hydrogen in the MIDREX process has the potential to become one of the
43 cornerstones of the global strategy to the decarbonization of ISI [23].

44 Although there exists a promising pathway for the low-carbon transformation of ISI through
45 the HDRI-EAF route and green hydrogen production, economic feasibility remains critical
46 to the development of this pathway, especially when using 100% hydrogen. The viability of
47 this pathway largely hinges on the costs associated with hydrogen production and the related
48 CO₂ emissions. The renewable hydrogen-based steelmaking system (RHSS), integrated with
49 renewable energy generation, green hydrogen production, and steelmaking processes, represents
50 an innovative paradigm of energy systems. The increasing maturity of related technologies, such
51 as green hydrogen production and hydrogen-based direct reduction of iron ore, is presenting
52 encouraging opportunities to enhance the development of RHSS and expand its market presence
53 consequently. Establishing expansion planning strategies that account for system evolution is

54 essential to optimize the long-term energy and economic efficiency of RHSS.

55 *1.2. Literature review*

56 Previous research on the optimal planning of energy systems are focused on the co-optimization
 57 of investment and operational strategies by a bi-level planning structure to achieve the lowest
 58 total cost or the highest profit [24, 25, 26].

59 Some researchers have explored investment planning on equipment capacity of RHSS. For
 60 instance, Ref.[27] uses a linear cost-minimization model with hourly resolution to determine
 61 the cost-optimal operation and sizing of RHSS units. Ref.[28] addresses system design and
 62 operational logic to ensure a consistent mass flow rate of hydrogen. Life cycle assessments
 63 (LCA) are commonly used to evaluate the levelized cost of crude steel (LCOCS). Ref.[29]
 64 emphasizes the impact of electricity prices and scrap steel usage on LCOCS. Ref.[30] further
 65 extends this analysis by considering the impact of the day-ahead electricity market on LCOCS.
 66 Other aspects of studies address renewable energy and electrolysis capacity requirements for
 67 the HDRI-EAF route, as discussed in Ref.[31, 32].

68 While most research considers current techno-economic parameters in designing optimal
 69 capacity investments, strategies for future expansion planning are less thoroughly investigated
 70 [33]. Considering the swift changes in techno-economic parameters due to technological ad-
 71 vances and market growth, developing a dynamic expansion planning model is essential to
 72 construct a rational planning strategy that ensures the economically and environmentally effi-
 73 cient development of RHSS.

74 To the best of our knowledge, the single-stage approach (SSA) and the perfect-sight ap-
 75 proach (PSA) are typical approaches for capacity investment planning of energy systems. The
 76 key characteristics of these two approaches are summarized in Table 1.

Table 1: Collection of literature on planning strategies of energy systems, indicating approaches and the MSEP model involvement. 'N/A' denotes not applicable, and '-' indicates data not provided.

Ref	System Type	Planning Horizon	Approach	Objective Function	MSEP Model Involvement
[30]	Hydrogen-based steel-making system	20 years	SSA	Minimization of the levelized cost of production.	N/A
[34]	Integrated electricity-heat-cold system	-	SSA	Minimization of the total annual cost considering CVaR.	N/A
[35]	Integrated electricity-hydrogen system	20 years	SSA	Minimization of the levelized cost of hydrogen.	N/A
[36]	Isolated hybrid AC/DC microgrids	-	SSA	Minimization of the total annual cost.	N/A
[37]	Hydrogen-electricity integrated systems	10 years	SSA	Minimization of the total annual cost.	N/A
[38]	Active distribution network	26 years	PSA	Minimization of the net present value of investment and operational costs.	√ (2 stages)
[39]	Electric power and natural gas systems	15 years	PSA	Minimization of the operating costs of the electric power and natural gas systems.	√ (3 stages)
[40]	Integrated electricity-heat-cold system	20 years	PSA	Minimization of the total annual costs of one representative year.	√ (4 stages)
[41]	Integrated electricity-gas-heat system	10 years	PSA	Minimization of the total annual costs.	√ (5 stages)

77 However, SSA relies on a single foresight horizon during the planning process, potentially
78 leading to redundant initial equipment capacity and substantial upfront investment costs [42].
79 For energy transitions over decades or even centuries, the multi-stage expansion planning
80 (MSEP) model is constructed to achieve better source-load matching and improve the eco-
81 nomic efficiency of long-term investment decisions by considering the construction sequence
82 and updates of techno-economic parameters [43]. PSA assumes that investors have perfect
83 foresight of the planning horizon, allowing optimization of both operating and investment de-
84 cisions throughout the planning horizon. However, as the expansion planning model for energy
85 systems is becoming increasingly challenging due to the growing complexity of system structures
86 and the longer planning horizons, the optimization model of PSA is burgeoned with large-scale
87 variables and constraints and is hard to solve within a reasonable time frame. Table 1 presents
88 a collection of literature on planning strategies of energy systems, indicating approaches and
89 the MSEP model involvement.

90 To overcome the limitations of SSA that may lead to suboptimal investment decisions and
91 the computational complexity of PSA, it is imperative to adopt a practical approach to reduce
92 the computational effort of the model. The rolling-horizon approach (RHA) addresses the
93 complexity of multi-stage optimization problems by implementing a temporal decomposition
94 strategy that simplifies the underlying temporal structure of the problem [44]. RHA starts the
95 optimization process with a finite foresight horizon, solving the problem iteratively by adapting
96 to a progressively displaced planning horizon and applying only the decisions relevant to the
97 current stage. By using a fix-and-update algorithm, RHA generates sequential optimization
98 decisions over the entire planning horizon, thereby reducing the computational effort.

99 *1.3. Research gap and contribution*

100 In summary, the existing literature applies a range of approaches to the planning strategies of
101 RHSS. However, there remains a noticeable gap in the systematic and comprehensive discussion
102 of expansion planning strategies for RHSS. By answering the question “What is the optimization
103 structure of the multi-stage expansion planning model of RHSS considering the construction
104 sequence and dynamic techno-economic parameters over the planning horizon, and how can this
105 model be solved accurately and efficiently?”, this study aims to develop a multi-stage expansion
106 planning model for RHSS and propose a rolling-horizon approach to balance the complexity and
107 feasibility of optimization, thereby providing a practical solution for the multi-stage expansion
108 planning of RHSS. The research framework of this study is illustrated in Fig. 1.

109 The main contributions of this study are threefold:

- 110 • Develop a multi-stage expansion model for RHSS, considering the construction sequence
111 and dynamic techno-economic parameters over the planning horizon from 2025 to 2050,
112 which provides rational capacity investment strategies to ensure the long-term economic
113 sustainability in both the investment and operation of RHSS.
- 114 • Propose a rolling-horizon approach to address the complexity of the optimization model
115 by segmenting the MSEP model into sequential sub-problems. This approach aims to
116 reduce the computational effort without sacrificing accuracy, thereby providing a practical
117 solution.
- 118 • Conduct sensitivity analysis to assess the impact of uncertainty in techno-economic pa-
119 rameters on the planning results. Meanwhile, perform robustness analysis under various
120 load growth scenarios to evaluate the applicability of RHA.

121 The structure of the rest of the paper is organized as follows: Section 2 presents the MSEP
 122 model of RHSS and Section 3 introduces the schematic of RHA for solving the MSEP model and
 123 the algorithmic steps involved. The practical implications of the proposed approach through
 124 case studies are illustrated in Section 4. Section 5 provides conclusions and suggestions for
 125 future work.

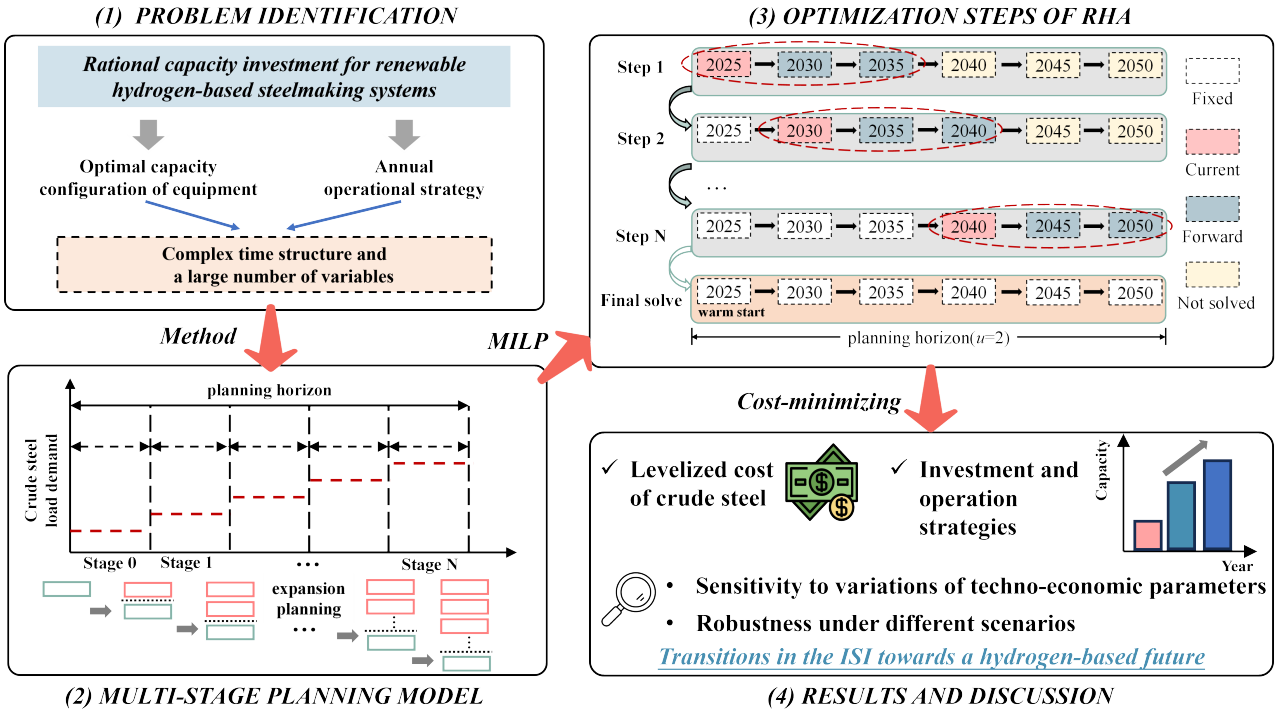


Fig. 1. The research framework of this study.

126 2. Problem definition and mathematical formulation

127 This section presents the MSEP model for minimizing the levelized cost of crude steel
 128 (LCOCS) of RHSS over the planning horizon, which determines the optimal capacity configu-
 129 ration of equipment and operating strategies to meet the system load requirements.

130 Besides, the MSEP model incorporates dynamic techno-economic parameters through a
 131 time-varying framework that updates equipment costs, technological advancements, and eco-
 132 nomic factors at each planning stage. This approach ensures that the sequence of construction
 133 activities align with both immediate and long-term system goals, optimizing resource deploy-
 134 ment and adapting to changing conditions.

135 2.1. Process description

136 As depicted in Fig. 2, RHSS allows the coupling of renewable electricity and the steel
 137 production process, integrating with renewable energy generation, green hydrogen production,
 138 hydrogen storage, direct reduction of iron ore, and steelmaking processes, which could be
 139 regarded as the “power to steel” conversion pathway.

140 Precisely, various RES such as photovoltaic (PV) and wind turbines (WT) are utilized by the
 141 system alongside conventional grid electricity. The power grid (PG) provides supplementary
 142 support to compensate for the intermittency of RES, ensuring a reliable electricity supply.
 143 Hydrogen is produced by electrolysis (EL), which is considered to be a polymer electrolyte

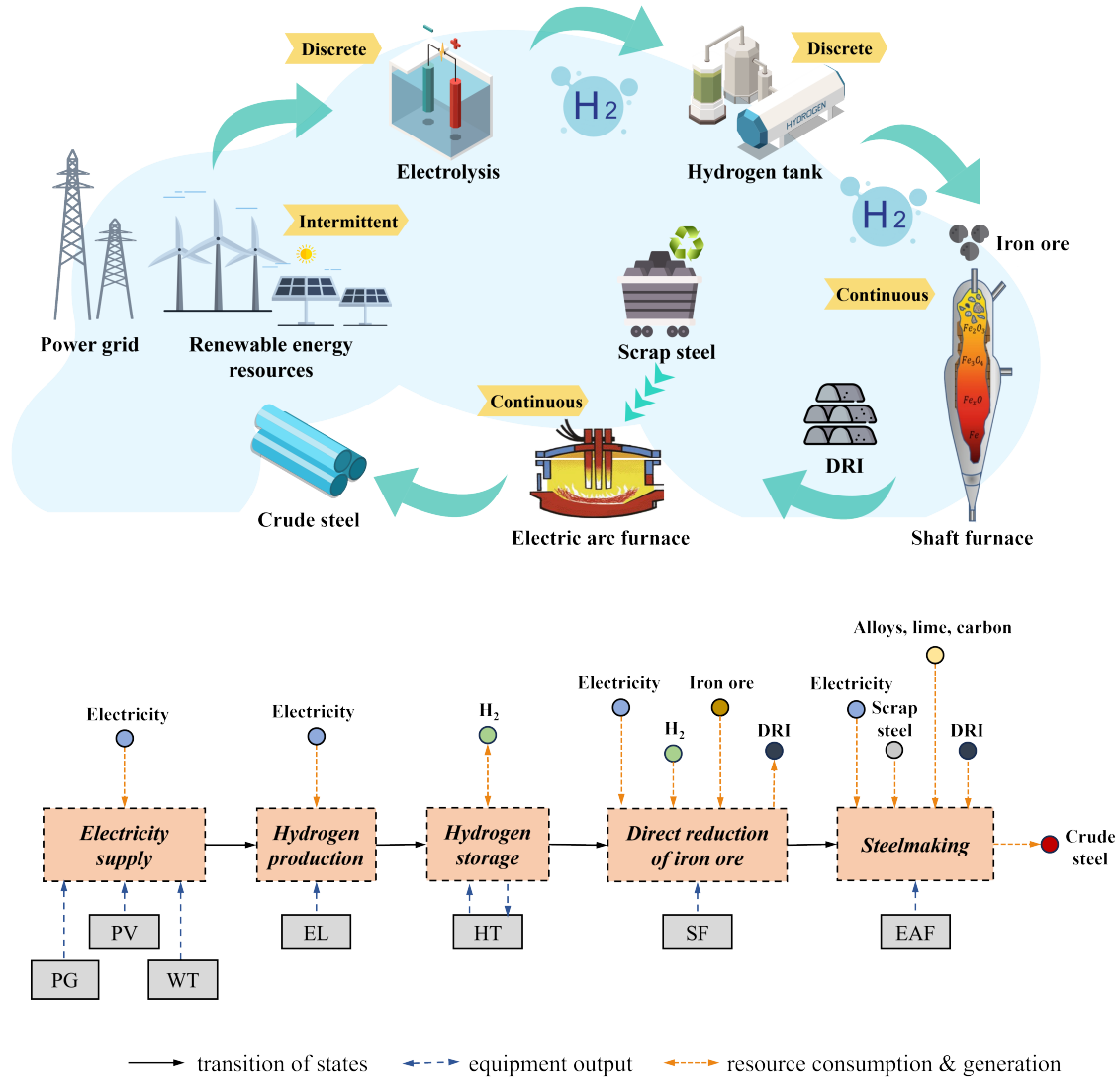


Fig. 2. The framework of RHSS

144 membrane (PEM) in this study. The hydrogen tank (HT) stores hydrogen for subsequent use
 145 in the steelmaking process, which manages the intermittent supply of hydrogen and the constant
 146 demand in downstream steelmaking processes. Hydrogen is then fed to the SF for direct iron
 147 ore reduction. The process culminates in the conversion of direct reduced iron (DRI) into steel
 148 in the EAF, thus completing the "power to steel" pathway.

149 2.2. Model assumption

150 Based on the process description above, the following assumptions are made for the MSEP
 151 model of RHSS:

- 152 1) Each planning stage is represented by a single year of each stage, the investment decision
 153 is made at the beginning of each planning stage [39].
- 154 2) The crude steel production of RHSS is greater than or equal to its rated production
 155 demand.
- 156 3) All material flows within the production cycle must adhere to the law of conservation of
 157 mass.
- 158 4) There is no product transportation time and no shadow product costs.

2.3. Objective function

The optimization objective of the MSEP model is to minimize the total cost and LCOCS of RHSS are over the planning horizon. This model is structured as a bi-level system (Fig. 3), where the upper level is dedicated to investment decision-making concerning the capacity configuration of equipment and the lower level focuses on operational strategies. The upper and lower-level problems are intricately interconnected and can be collaboratively formulated into a mixed-integer linear programming (MILP) model.

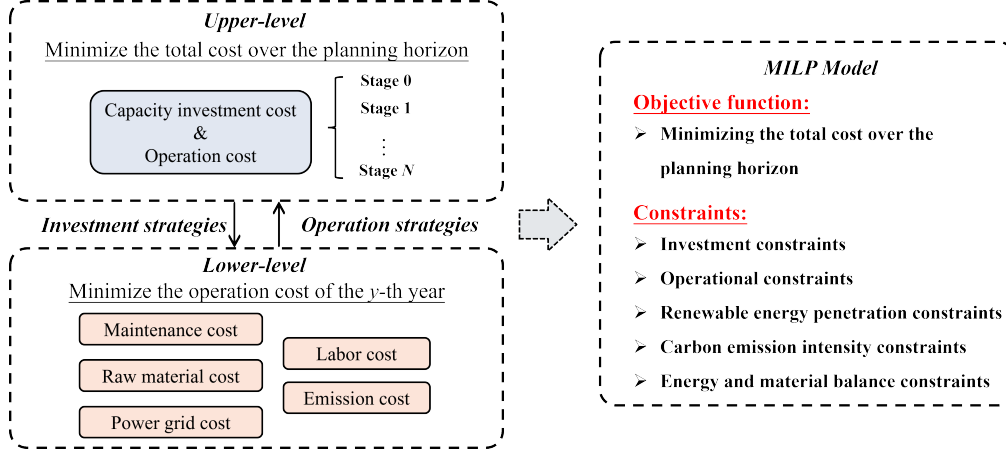


Fig. 3. The bi-level structure of the MSEP model of RHSS

The MSEP model divides the planning horizon (total of n years) into N planning stages. Capacity investments are made at the beginning of each planning stage, while operational decisions are made annually. $y \in \{1, 2, \dots, n\}$ denotes the specific planning year.

Capacity investment costs are the costs associated with each type of equipment over the N planning stages. The future capital is discounted to the present value by a discount factor r , where r is set at 4%.

$$R^y = (1 + r)^{-y} \quad \forall y \in Y \quad (1)$$

$$C_i^{\text{inv},m} = c_i^{\text{inv},m} V_i^m \quad \forall i \in N, \forall m \in M \quad (2)$$

$$C_i^{\text{inv}} = \sum_{m \in M} C_i^{\text{inv},m} \quad \forall i \in N, \forall m \in M \quad (3)$$

Therefore, the objective function of the MSEP model can be described as follows:

$$\min f = \frac{\sum_{i \in N} R^i C_i^{\text{inv}} + \sum_{y \in Y} R^y C_y^{\text{ope}} - F^{\text{rv}}}{\sum_{i \in N} (Y_i \times \sum_{s \in S} (D_s \times \sum_{t \in T} S_{i,s,t}^{\text{eaf}}))} \quad \forall i \in N, \forall y \in Y \quad (4)$$

where R^i is the discount factor of the beginning year of stage i .

The operational costs encompass maintenance, raw material, power grid, labor, and emissions costs. To accurately capture the operational dynamics across different seasons, three typical days are selected to represent the system's operational characteristics during summer, winter, and transitional seasons. The operational costs for the y -th year ($y \in$ stage i) are calculated as the sum of the costs of these three representative days, which can be expressed as follows:

$$C_y^{\text{ope}} = C_y^{\text{mai}} + C_y^{\text{raw}} + C_y^{\text{grid}} + C_y^{\text{lab}} + C_y^{\text{emi}} \quad \forall i \in N, \forall y \in Y \quad (5)$$

$$C_y^{\text{mai}} = \sum_{m \in M} c_i^{\text{mai},m} C_i^{\text{inv},m} \quad \forall m \in M, \forall y \in Y \quad (6)$$

$$C_y^{\text{raw}} = \sum_{s \in S} \left(D_s \times \sum_{z \in Z} \sum_{t \in T} c_z Q_z S_{i,s,t}^{\text{eaf}} \right) \quad (7)$$

$$C_y^{\text{grid}} = \sum_{s \in S} \left(D_s \times \sum_{t \in T} c_t^{\text{TOU}} P_{i,s,t}^{\text{grid}} \right) \quad (8)$$

$$C_y^{\text{lab}} = \sum_{s \in S} \left(D_s c^{\text{lab}} \times \sum_{t \in T} S_{i,s,t}^{\text{eaf}} \right) \quad (9)$$

$$C_y^{\text{emi}} = \sum_{s \in S} \left(D_s \times \sum_{t \in T} c^{\text{tax}} \left(\varepsilon^{\text{grid}} P_{i,s,t}^{\text{grid}} + \varepsilon^{\text{iron}} Q_{i,s,t}^{\text{iron}} + \varepsilon^{\text{eaf}} S_{i,s,t}^{\text{eaf}} \right) \right) \quad (10)$$

180 In (5), C_y^{mai} , C_y^{raw} , C_y^{grid} , C_y^{lab} , and C_y^{emi} denote the maintenance, raw material, power
 181 grid, labor, and emission costs of the y -th year, respectively. Maintenance costs in (6) are
 182 calculated as the sum of the maintenance costs for each type of equipment. Raw material costs
 183 in (7) consist of the costs of raw materials (alloys, lime, iron ore, carbon, and scrap steel)
 184 consumed in the steelmaking process. Power grid costs in (8) are related to the Time-of-Use
 185 (TOU) electricity price and electricity purchased from the grid. Labor costs in (9) are positively
 186 correlated with the amount of crude steel production.

187 Emissions are divided into direct and indirect emissions, the former of which come from the
 188 steelmaking process of EAF and the operation of the power grid, while the latter is associated
 189 with upstream processes, mainly from the iron ore production process. In (10), $\varepsilon^{\text{grid}}$, $\varepsilon^{\text{iron}}$,
 190 and ε^{eaf} denote the grid-average emission factor (EF), iron ore production EF and crude steel
 191 production EF, respectively.

192 Regarding the financial assessment of equipment, the net residual value at the end of the
 193 planning horizon is calculated by applying a discount rate δ_m (set at 6%). The straight-line
 194 method (SLM) of depreciation [45] is used to calculate the depreciation rate of the equipment,
 195 assuming that the value of the equipment declines uniformly over its expected technical life.

$$F^{\text{rv}} = \sum_{m \in M} \sum_{i \in N} \left(\left(C_i^{\text{inv},m} - \sum_{y=1}^{Y_i^m} C_i^{\text{dep},m} \right) \times R^n \right) \quad \forall i \in N, \forall m \in M, \forall y \in Y \quad (11)$$

$$C_i^{\text{dep},m} = C_i^{\text{inv},m} (1 - \delta) / \lambda_m \quad \forall i \in N, \forall m \in M \quad (12)$$

196 2.4. Constraints

197 RHSS is subject to a series of constraints to ensure the feasibility of the investment decisions,
 198 operational strategies and system performance. The MSEP model of RHSS needs to meet the
 199 following constraints.

200 2.4.1. Multi-stage investment logic constraints

$$V_i^m \geq V_i^{m,\text{min}} \quad \forall i \in N, \forall m \in M \quad (13)$$

$$V_i^m \leq V_i^{m,\max} \quad \forall i \in N, \forall m \in M \quad (14)$$

$$V_i^m \geq V_{i-1}^m \quad \forall i \in N, \forall m \in M \quad (15)$$

$$V_i^m \leq V_{i-1}^m + V_i^{m,\max} \quad \forall i \in N, \forall m \in M \quad (16)$$

201 Constraints (13)-(14) ensure that the capacity configuration of each equipment type at each
 202 stage is within the minimum and maximum capacity limits, and the capacity of each equipment
 203 type at each stage should be positive. Constraints (15)-(16) describe the capacity investment
 204 logic between different stages.

205 2.4.2. Discrete-operating equipment constraints

206 EL and HT are examples of discrete-operating equipment that can accommodate fluctua-
 207 tions in RES efficiently and optimize the energy exchange between hydrogen production and
 208 other processes in RHSS, facilitating the integration of renewable energy and the steelmaking
 209 process. The operational constraints of EL and HT are formulated as follows:

210 For the operational constraints of the k -th electrolyzer module ($k = 0, 1, \dots, K$), where K
 211 represents the total number of EL modules planned at stage i , the constraints are formulated
 212 as follows:

$$V_i^{\text{el},k} \eta_{\min}^{\text{el}} \leq P_{i,s,t}^{\text{el},k} \leq V_i^{\text{el},k} \eta_{\max}^{\text{el}} \quad \forall i \in N, \forall s \in S, \forall t \in T \quad (17)$$

$$|P_{i,s,t}^{\text{el},k} - P_{i,s,t-1}^{\text{el},k}| \leq \Delta P^{\text{el}} \quad \forall i \in N, \forall s \in S, \forall t \in T \quad (18)$$

$$G_{i,s,t}^{\text{el},k} = P_{i,s,t}^{\text{el},k} / \omega^{\text{el}} \quad \forall i \in N, \forall s \in S, \forall t \in T \quad (19)$$

$$s_{i,s,t}^{\text{el},k} - d_{i,s,t}^{\text{el},k} = u_{i,s,t}^{\text{el},k} - u_{i,s,t-1}^{\text{el},k} \quad \forall i \in N, \forall s \in S, \forall t \in T \quad (20a)$$

$$u_{i,s,1}^{\text{el},k} = u_{i,s,t}^{\text{el},k} \quad \forall i \in N, \forall s \in S, \forall t \in T \quad (20b)$$

$$s_{i,s,t}^{\text{el},k} \leq 1 - s_{i,s,t-1}^{\text{el},k} \quad \forall i \in N, \forall s \in S, \forall t \in T \quad (20c)$$

$$d_{i,s,t}^{\text{el},k} \leq d_{i,s,t-1}^{\text{el},k} \quad \forall i \in N, \forall s \in S, \forall t \in T \quad (20d)$$

$$\sum_{t \in T} s_{i,s,t}^{\text{el},k} \leq S_{\max}^{\text{el}} \quad \forall i \in N, \forall s \in S, \forall t \in T \quad (20e)$$

$$\sum_{t \in T} d_{i,s,t}^{\text{el},k} \leq D_{\max}^{\text{el}} \quad \forall i \in N, \forall s \in S, \forall t \in T \quad (20f)$$

213 Constraints (17)-(18) describe the maximum and minimum operating ratios and ramp lim-
 214 itation of EL. Constraint (19) denotes the efficiency in converting electricity to hydrogen.
 215 Constraints (20a)-(20f) describe the start-stop principle of EL.

216 Considering the complexity of modeling the operational constraints of multiple EL modules
 217 by the traditional Unit Commitment (UC) model, we adopt the Clustered Unit Commitment
 218 (CUC) model to aggregate multiple EL modules into the EL cluster, and the binary vari-
 219 ables (on/off state, start-up operation, and shut-down operation) can be simplified by integer
 220 variables [46]. Taking the on/off state variables as an example, the comparison between the
 221 traditional UC model and the CUC model of EL modules is shown in Fig. 4.

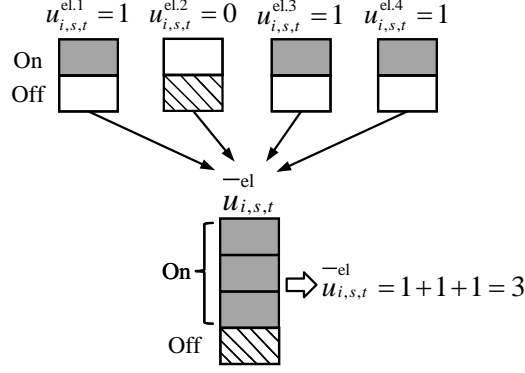


Fig. 4. Comparison between the traditional UC model and the CUC model for multiple EL modules

222 The binary variables in constraint (20a)-(20f) can be adjusted to the form of constraint
 223 (21a)-(21f), to describe the start-stop principle of the EL cluster:

$$\bar{s}_{i,s,t}^{\text{el}} - \bar{d}_{i,s,t}^{\text{el}} = \bar{u}_{i,s,t}^{\text{el}} - \bar{u}_{t-1}^{\text{el}} \quad \forall i \in N, \forall s \in S, \forall t \in T \quad (21a)$$

$$\bar{u}_{i,s,1}^{\text{el}} = \bar{u}_{i,s,t}^{\text{el}} \quad \forall i \in N, \forall s \in S, \forall t \in T \quad (21b)$$

$$\bar{s}_{i,s,t}^{\text{el}} \leq K - \bar{s}_{i,s,t-1}^{\text{el}} \quad \forall i \in N, \forall s \in S, \forall t \in T \quad (21c)$$

$$\bar{d}_{i,s,t}^{\text{el}} \leq \bar{d}_{i,s,t-1}^{\text{el}} \quad \forall i \in N, \forall s \in S, \forall t \in T \quad (21d)$$

$$\sum_{t \in T} \bar{s}_{i,s,t}^{\text{el}} \leq K S_{\max}^{\text{el}} \quad \forall i \in N, \forall s \in S, \forall t \in T \quad (21e)$$

$$\sum_{t \in T} \bar{d}_{i,s,t}^{\text{el}} \leq K D_{\max}^{\text{el}} \quad \forall i \in N, \forall s \in S, \forall t \in T \quad (21f)$$

224 HT provides a flexible distribution of hydrogen consumption over time. The operational
 225 constraints of HT are detailed as follows:

$$0 \leq G_{i,s,t}^{\text{ht.c}} \leq V_i^{\text{ht}} \eta_{\max}^{\text{ht}} \quad \forall i \in N, \forall s \in S, \forall t \in T \quad (22)$$

$$0 \leq G_{i,s,t}^{\text{ht.d}} \leq V_i^{\text{ht}} \eta_{\max}^{\text{ht}} \quad \forall i \in N, \forall s \in S, \forall t \in T \quad (23)$$

$$E_{i,s,t+1}^{\text{ht}} = E_{i,s,t}^{\text{ht}} (1 - \delta^{\text{ht}}) + \frac{G_{i,s,t}^{\text{ht.c}} \omega^{\text{ht.c}}}{V_i^{\text{ht}}} - \frac{G_{i,s,t}^{\text{ht.d}}}{\omega^{\text{ht.d}} V_i^{\text{ht}}} \quad \forall i \in N, \forall s \in S, \forall t \in T \quad (24)$$

$$v_{i,s,t}^{\text{ht.c}} + v_{i,s,t}^{\text{ht.d}} \leq 1 \quad \forall i \in N, \forall s \in S, \forall t \in T \quad (25)$$

$$E_{i,s,1}^{\text{ht}} = E_{i,s,T}^{\text{ht}} \quad \forall i \in N, \forall s \in S \quad (26)$$

226 Constraints (22)-(23) describe the maximum and minimum hydrogen charging and dis-
 227 charging power ratios of HT. Constraint (24) denotes the relationship between the charg-
 228 ing/discharging power and the state of charge (SOC) of HT, considering both efficiency factors
 229 and the self-discharge rate. Additionally, constraints (25) - (26) represent the start-stop prin-
 230 ciple of HT, that charging and discharging processes cannot be performed simultaneously, and

231 the start and end SOC must be identical each day to maintain the daily energy balance.

232 2.4.3. Continuous-operating equipment constraints

233 SF and EAF are categorized as continuous-operating equipment in RHSS [27]. Both SF and
 234 EAF must operate without interruptions to ensure a consistent production flow and to meet
 235 the high stability requirements of crude steel production. The operational constraints of SF
 236 and EAF are detailed as follows:

237 In the SF, iron ore pellets are reduced to DRI using hydrogen as the reducing agent. This
 238 study assumes that the SF is integrated with a pre-heating stage. The operational constraints
 239 of the SF are as follows:

$$V_i^{\text{sf}} \eta_{\min}^{\text{sf}} \leq I_{i,s,t}^{\text{sf}} \leq V_i^{\text{sf}} \eta_{\max}^{\text{sf}} \quad \forall i \in N, \forall s \in S, \forall t \in T \quad (27)$$

$$G_{i,s,t}^{\text{sf}} = I_{i,s,t}^{\text{sf}} / \omega^{\text{sf.DRI}} \quad \forall i \in N, \forall s \in S, \forall t \in T \quad (28a)$$

$$P_{i,s,t}^{\text{sf}} = I_{i,s,t}^{\text{sf}} / \omega^{\text{sf.e}} \quad \forall i \in N, \forall s \in S, \forall t \in T \quad (28b)$$

240 Constraint (27) describes the maximum and minimum reduction power ratios of SF. Con-
 241 straints (28a)-(28b) denote the relationship between hydrogen and power consumption and the
 242 DRI production of SF, which is determined by the reduction and power consumption efficiency.

243 EAF can take any fraction of sponge iron (from 0% to 100%) into crude steel production and
 244 is the most common way of producing secondary steel from scrap steel [16]. The operational
 245 constraints of the EAF, which ensure its efficiency and adaptability in handling different input
 246 raw materials, are as follows:

$$V_i^{\text{eaf}} \eta_{\min}^{\text{eaf}} \leq S_{i,s,t}^{\text{eaf}} \leq V_i^{\text{eaf}} \eta_{\max}^{\text{eaf}} \quad \forall i \in N, \forall s \in S, \forall t \in T \quad (29)$$

$$S_{i,s,t}^{\text{eaf}} = I_{i,s,t}^{\text{sf}} / \omega^{\text{eaf.DRI}} + Q_{i,s,t}^{\text{scrap}} / \omega^{\text{eaf.scrap}} \quad \forall i \in N, \forall s \in S, \forall t \in T \quad (30a)$$

$$S_{i,s,t}^{\text{eaf}} = P_{i,s,t}^{\text{eaf}} / \omega^{\text{eaf.e}} \quad \forall i \in N, \forall s \in S, \forall t \in T \quad (30b)$$

247 Constraint (29) describes the maximum and minimum crude steel production ratios of EAF.
 248 Constraints (30a) denote the relationship between the DRI and scrap steel consumption with
 249 the production of crude steel in EAF. Constraint (30b) represents the power consumption of
 250 EAF, which is determined by the power consumption efficiency.

251 2.4.4. Energy and material balance constraints

252 The energy and material balance constraints are critical for managing the interactions be-
 253 tween the various energy and material flows within the system, which are shown as follows:

$$P_{i,s,t}^{\text{wt}} + P_{i,s,t}^{\text{pv}} + P_{i,s,t}^{\text{grid}} = P_{i,s,t}^{\text{el}} + P_{i,s,t}^{\text{sf}} + P_{i,s,t}^{\text{eaf}} \quad \forall i \in N, \forall s \in S, \forall t \in T \quad (31)$$

$$G_{i,s,t}^{\text{el}} + G_{i,s,t}^{\text{ht.d}} = G_{i,s,t}^{\text{ht.c}} + G_{i,s,t}^{\text{sf}} \quad \forall i \in N, \forall s \in S, \forall t \in T \quad (32)$$

$$S_{i,s,t}^{\text{eaf}} \geq S_{i,s,t}^{\text{cs}} \quad \forall i \in N, \forall s \in S, \forall t \in T \quad (33)$$

254 Constraints (31)-(33) represent the energy and material balance constraints among differ-
 255 ent energy carriers and materials in RHSS. It should be noted that while the electricity and

256 hydrogen balance constraints should be strictly satisfied, the steel balance constraint can be
 257 relaxed to ensure a stable steelmaking process.

258 2.4.5. Renewable energy penetration constraints

259 The renewable energy penetration (REP) constraints at each planning stage are designed
 260 to ensure that a certain percentage of use from RES, facilitating the gradual increase of REP
 261 as part of the system's sustainability objectives. The constraints are formulated as follows:

$$0 \leq P_{i,s,t}^{\text{wt}} \leq V_i^{\text{wt}} P_{i,s,t}^{\text{wt.N}} \quad \forall i \in N, \forall s \in S, \forall t \in T \quad (34a)$$

$$0 \leq P_{i,s,t}^{\text{pv}} \leq V_i^{\text{pv}} P_{i,s,t}^{\text{pv.N}} \quad \forall i \in N, \forall s \in S, \forall t \in T \quad (34b)$$

$$\frac{\sum_{s \in S} (D_s \times \sum_{t \in T} (P_{i,s,t}^{\text{wt}} + P_{i,s,t}^{\text{pv}}))}{\sum_{s \in S} (D_s \times \sum_{t \in T} (P_{i,s,t}^{\text{wt}} + P_{i,s,t}^{\text{pv}} + P_{i,s,t}^{\text{grid}}))} \geq \rho_i \quad \forall i \in N, \forall s \in S, \forall t \in T \quad (35)$$

262 Constraints (34a)-(34b) describe the maximum wind and solar power generation capacity
 263 of WT and PV at each planning stage. Constraint (35) denotes the REP rate at each planning
 264 stage.

265 2.4.6. CO₂ intensity constraints

266 The CO₂ intensity constraints at each planning stage aim to regulate and limit the CO₂
 267 emissions per production unit. By setting these limits, the model can support the system's
 268 transition towards lower CO₂ emissions. The constraints are formulated as follows:

$$\sum_{s \in S} \left(D_s \times \sum_{t \in T} \left(\varepsilon^{\text{grid}} P_{i,s,t}^{\text{grid}} + \varepsilon^{\text{iron}} Q_{i,s,t}^{\text{iron}} + \varepsilon^{\text{eaf}} S_{i,s,t}^{\text{eaf}} \right) \right) \leq \varepsilon_i \quad \forall i \in N, \forall s \in S, \forall t \in T \quad (36)$$

269 Constraint (36) describes the CO₂ intensity at each planning stage, which is determined by
 270 the EF of the power grid, iron ore production, and crude steel production.

271 3. Rolling-horizon approach for solving the MSEP model

272 The MSEP model discussed in Section 2 is a mixed-integer linear programming (MILP)
 273 model with a complex time structure and a large number of variables, including continuous,
 274 integer, and binary types. While NP-hard problems are computationally solvable using existing
 275 commercial solvers, achieving global optimality within a reasonable time frame often proves
 276 challenging and may even lead to memory overflow issues.

277 Therefore, in this section, RHA is proposed to enhance the efficiency of the solution process.
 278 RHA segments the model into sequential portions, updating the information for subsequent
 279 stages as it progresses. The general formulation of RHA is introduced in Section 3.1. Section 3.2
 280 then compares the algorithm steps of RHA with SSA and PSA. Finally, Section 3.3 details the
 281 implementation of RHA to solve the MSEP model.

282 3.1. General formulation of RHA

283 RHA is characterized by its capability to manage the complexities of optimization problems
 284 that incorporate extensive time structures through temporal decomposition. That is, to divide
 285 a large-scale problem into a series of smaller-scale sub-problems, which can be solved with

286 a much shorter computation time. As each sub-problem is solved sequentially, information
 287 from completed stages is incorporated into subsequent stages, ensuring solution continuity and
 288 consistency.

289 While RHA does not necessarily guarantee global optimality, its iterative nature allows
 290 for adjustments across iterations. By setting an appropriate foresight horizon and fixing only
 291 the decisions of the current stage, it iteratively optimizes the decisions for upcoming stages,
 292 correcting deviations and refining the overall solution.

293 The MSEP model is first formulated as a series of single-stage planning problems P_i ($i =$
 294 $0, 1, \dots, N$). P_i aims to minimize the total cost of each stage, which is formulated as follows:

$$\begin{aligned} \min \quad & f_i(x_i) \\ \text{s.t.} \quad & g_i(\xi_i, x_i, \vartheta_i) \leq 0 \\ & (\xi_i, x_i, \vartheta_i) \in \Xi_i \times X_i \times \Theta_i \end{aligned} \quad (37)$$

295 where ξ_i ($\xi_i \in \Xi_i$) represent the initial state variables, ϑ_i ($\vartheta_i \in \Theta_i$) denote final state variables,
 296 and x_i ($x_i \in X_i$) represent internal variables.

297 The initial state variables and final state variables link the current stage to the previous
 298 and subsequent stages, and the set of final state variables of the current stage is included in the
 299 set of initial state variables of the following stage. The objective function f_i depends only on
 300 the internal variables x_i , while ξ_i , g_i and ϑ_i are constrained by the related constraints between
 301 the stages, ensuring continuity and correlation between the stages.

302 Then, a finite foresight planning problem $P_{i,\mu}$ ($\mu \in \mathbb{N}_0, \mu + i \leq N$) is defined as a combi-
 303 nation of multiple single-stage planning problems, which starts from stage i and comprises a
 304 μ -stage foresight horizon. $P_{i,\mu}$ is adhered to a set of constraints that ensure the feasibility of
 305 solutions at each stage within the planning horizon, which is formulated as follows:

$$\begin{aligned} \min \quad & \sum_{j=i}^{i+\mu} f_j(x_j) \\ \text{s.t.} \quad & g_j(\xi_j, x_j, \vartheta_j) \leq 0 \quad \forall j \in \{i, \dots, i + \mu\} \\ & \xi_j = \vartheta_{j-1} \quad \forall j \in \{i + 1, \dots, i + \mu\} \\ & (\xi_j, x_j, \vartheta_j) \in \Xi_j \times X_j \times \Theta_j \quad \forall j \in \{i, \dots, i + \mu\} \end{aligned} \quad (38)$$

306 $P_{i,\mu}$ contains fewer variables and constraints than the original MSEP model, along with the
 307 iteration process of RHA, the resolution of the sub-problem $P_{i,\mu}^{\xi_i}$ is conducted to obtain the
 308 optimal decisions $(\xi_i, x_i, \vartheta_i)$. For instance, RHA solves $P_{0,\mu}$ to obtain the solution of stage 0,
 309 and then $(\xi_0, x_0, \vartheta_0)$ is fixed. After that, RHA solves $P_{1,\mu}$ to obtain the solution of stage 1, and
 310 then $(\xi_1, x_1, \vartheta_1)$ is fixed. This process is repeated until the final stage N is reached.

311 3.2. Comparison between SSA, PSA and RHA

312 This subsection presents a comparison between SSA, PSA, and RHA in terms of their
 313 algorithm steps and optimization strategies.

314 SSA focuses on solving a single-stage planning problem by considering only the parameters
 315 of the current stage, neglecting potential changes and trends in future stages. Thus, P_{SSA} can
 316 be considered as an intuitive formulation that can naturally be developed for the single-stage
 317 planning problem of RHSS. The formulation of the single-stage planning model for RHSS can
 318 be described as (39). Due to its limited foresight horizon, SSA often results in myopic decisions
 319 that can lead to initial capacity redundancy and waste of resources.

$$\begin{aligned}
(P_{SSA}) \quad \min \quad & f = \frac{R^i C_{i=0}^{\text{inv}} + R^y C_y^{\text{ope}} - F^{\text{rv}}}{\sum_{s \in S} (D_s \times \sum_{t \in T} S_{0,s,t}^{\text{eaf}})} \\
\text{s.t.} \quad & P_{0,s,t}^{\text{wt}} + P_{0,s,t}^{\text{pv}} + P_{0,s,t}^{\text{grid}} = P_{0,s,t}^{\text{el}} + P_{0,s,t}^{\text{sf}} + P_{0,s,t}^{\text{eaf}} \\
& G_{0,s,t}^{\text{el}} + G_{0,s,t}^{\text{ht.d}} = G_{0,s,t}^{\text{ht.c}} + G_{0,s,t}^{\text{sf}} \\
& S_{0,s,t}^{\text{eaf}} \geq S_{N,s,t}^{\text{cs}} \\
& 0 \leq P_{0,s,t}^{\text{wt}} \leq V_0^{\text{wt}} P_{0,s,t}^{\text{wt.N}} \\
& 0 \leq P_{0,s,t}^{\text{pv}} \leq V_0^{\text{pv}} P_{0,s,t}^{\text{pv.N}} \\
& \frac{\sum_{s \in S} (D_s \times \sum_{t \in T} (P_{0,s,t}^{\text{wt}} + P_{0,s,t}^{\text{pv}}))}{\sum_{s \in S} (D_s \times \sum_{t \in T} (P_{0,s,t}^{\text{wt}} + P_{0,s,t}^{\text{pv}} + P_{0,s,t}^{\text{grid}}))} \geq \rho_0 \\
& \sum_{s \in S} \left(D_s \times \sum_{t \in T} (\varepsilon^{\text{grid}} P_{0,s,t}^{\text{grid}} + \varepsilon^{\text{iron}} Q_{0,s,t}^{\text{iron}} + \varepsilon^{\text{eaf}} S_{0,s,t}^{\text{eaf}}) \right) \leq \varepsilon_0 \\
& \text{Constraints(17) - (19)} \\
& \text{Constraints(21a) - (30b)}
\end{aligned} \tag{39}$$

320 In contrast, PSA is designed to tackle the MSEP model by considering the interactions
321 between different stages over an extended planning horizon. On such problems, as the tem-
322 poral dimension increases, the complexity of the optimization problem grows exponentially.
323 Consequently, PSA is burgeoned with plenty of variables and constraints and is hard to solve
324 within a reasonable time frame.

325 Owing to the high computational cost discussed above, obtaining optimal solutions for the
326 MSEP model using PSA with state-of-the-art MILP solvers remains computationally challeng-
327 ing when the planning horizon is extended. RHA is proposed to address this issue by solving the
328 MSEP model in a sequence of steps, which streamlines the solution of large-scale optimization
329 problems by breaking them down into sequential segments, thus lower computational effort
330 is required to solve each sub-problem, Meanwhile, RHA enhances flexibility and adaptability
331 during the solution process by allowing the incorporation of new information and adjustments
332 as the model progresses, which facilitates more feasible and practical planning results.

333 3.3. Implementation of RHA for solving the MSEP model

334 The detailed optimization procedure of RHA for solving the MSEP model is illustrated in
335 Fig. 5. RHA optimizes the investment and operational strategies of each sub-problem, which
336 is formulated as a multi-stage planning problem with a foresight horizon of u stages. Then,
337 by iteratively solving the sub-problems, RHA updates the information for subsequent stages,
338 ensuring the continuity and consistency of the solution.

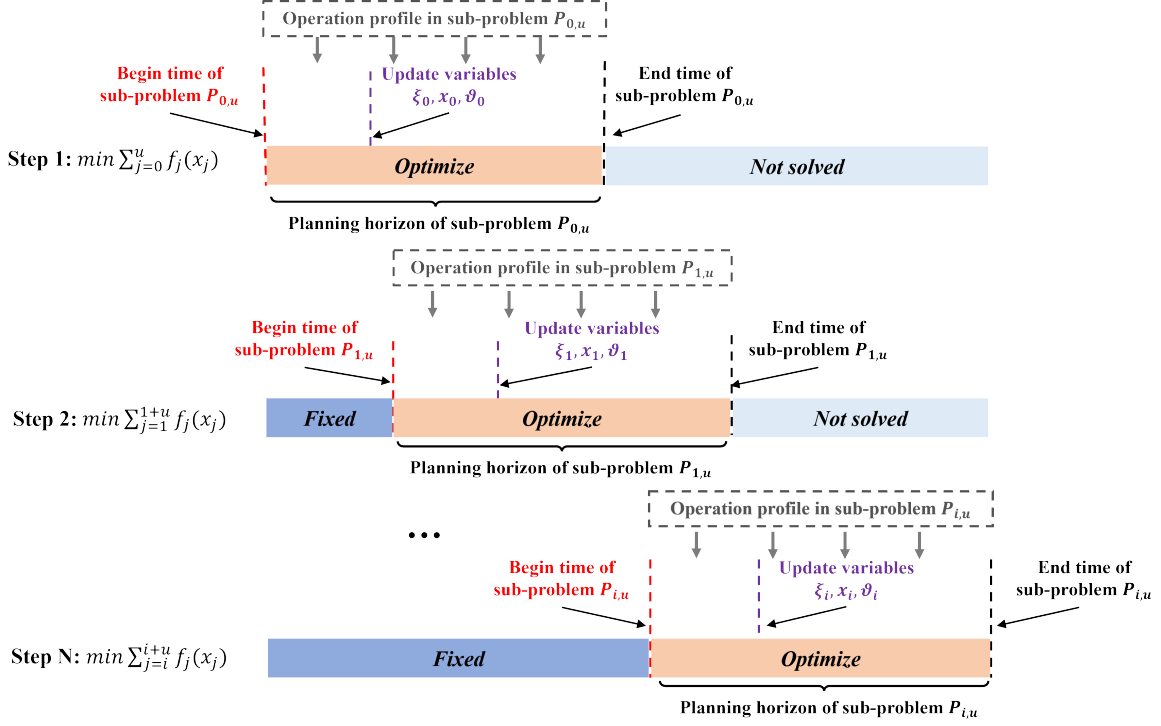


Fig. 5. Optimization procedure of RHA for solving the MSEP model

339 According to the optimization procedure described above, the algorithm of RHA for solving
 340 the MSEP model is summarized as follows:

Algorithm: Rolling-horizon approach for solving the MSEP model

- 1: **Input:** Initial state variables ξ_0 , planning horizon N , foresight horizon μ
 - 2: **Output:** Optimal solution for each stage
 - 3: **Initialization:** Set current stage $i = 0$
 - 4: **while** $i < N$ **do**
 - 5: Define sub-problem $P_{i,\mu}^{\xi_i}$ within horizon $[i, \min(i + \mu, N)]$
 - 6: Solve $P_{i,\mu}^{\xi_i}$ to obtain optimal decisions $(\xi_i, x_i, \vartheta_i)$
 - 7: Update variables: ξ_i, x_i, ϑ_i
 - 8: $i \rightarrow i + \mu$ // Advance to the next stage
 - 9: **if** $i + \mu > N$ **then**
 - 10: $\mu = N - i$ // Adjust horizon for the last stage
 - 11: **end if**
 - 12: Update parameters and constraints based on new information
 - 13: **end while**
 - 14: **Warm Start:** Utilize results $\{(\xi_i, x_i, \vartheta_i)\}_{i=0}^N$ to initiate a comprehensive optimization for operational strategies to obtain the overall optimal strategy.
-

341 **4. Case study**

342 This section presents case studies to demonstrate the performance of RHA for solving the
 343 MSEP model of RHSS illustrated in Section 2, in terms of accuracy and computational efficiency
 344 (Section 4.2), multi-stage expansion planning strategies (Section 4.3), and environmental impact

(Section 4.4), such as renewable energy penetration rate and CO₂ intensity. Furthermore, the sensitivity and robustness analysis of the proposed model are conducted in Section 4.5.

4.1. Basic settings

We develop a long-term planning framework for RHSS that covers a 25-year planning horizon from 2025 to 2050. We consider five investment stages within the planning horizon of 25 years. A 4-year operating stage follows each investment stage. Consequently, the associated techno-economic parameters and load demand at each stage are assumed to be constant. Since identifying the uncertainty of the parameters is out of this work's scope, we assume that the forecasting errors are negligible. The crude steel load demand is set to follow a linear growth trend, i.e.

$$L(i) = L_0 + \kappa i \quad i = 0, 1, 2, 3, 4 \quad (40)$$

where $L(i)$ represents the hourly load demand at stage i , L_0 is the initial load demand per hour (t_{cs}/h), and κ is the linear growth factor of the load demand (t_{cs}/h per stage). For the case study discussed in this paper, the initial load demand L_0 is set to 1 t_{cs}/h , with a growth factor κ of 2 t_{cs}/h per stage.

The assumptions of CAPEX (capital expenditure) and OPEX (operational expenditure) from 2025 to 2050 in this study are listed in Table A1, and other associated parameters are listed in Table A3. The WT and PV curves (in per unit values) for a typical metric year (TMY) and typical seasonal days are shown in Fig. A1. TOU electricity prices for each typical day are shown in Fig. A2. The numerical experiments are performed in Matlab2022A and solved by the commercial solver [47] on a personal computer with a 2.50GHz CPU and 32.0GB RAM.

4.2. Analysis of computational efficiency and accuracy

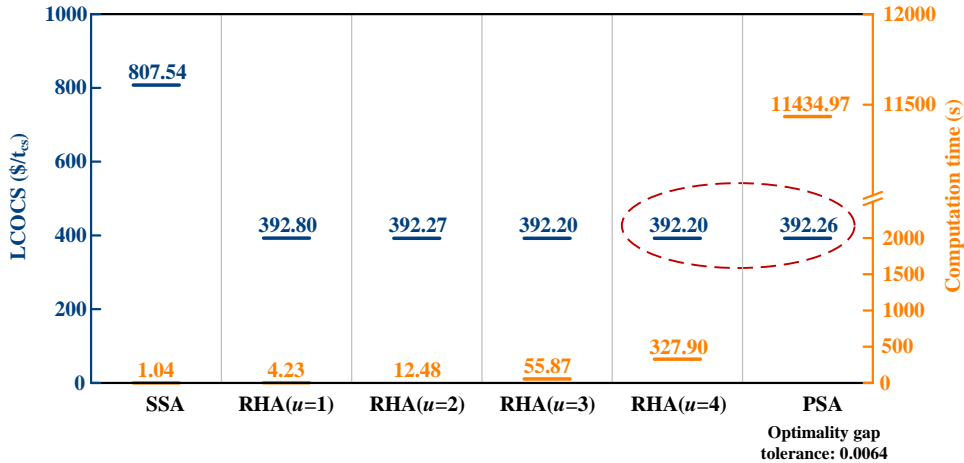


Fig. 6. Comparison of the optimal LCOCS and computation time using different approaches

The results comparing the optimal LCOCS and computation time for SSA, RHA, and PSA are shown in Fig. 6. The results show that while SSA has the lowest computational cost, due to its less complex one-step model, it leads to a myopic solution of 807.54 $\$/t_{cs}$, which is about twice the optimal solution of 392.20 $\$/t_{cs}$.

PSA and RHA provide more economically efficient solutions by an expansion planning strategy taking into account the construction sequence and dynamic techno-economic parameters. However, as the complexity of the MSEP model escalates, PSA may fail to provide solutions

373 within a reasonable time frame. It turns out that PSA cannot be solved for global optimality by
 374 Gurobi since the gap value remains at 0.64% after running for 11434 s , and an out-of-memory
 375 error occurred when the solution time exceeded 8 hours. Thus, at an optimality gap tolerance
 376 of 0.64%, PSA provides a suboptimal solution of 392.26 $\$/t_{cs}$, which is higher than the optimal
 377 LCOCS using RHA ($u=3/4$). Further experiments on the computation time of PSA are under
 378 the same optimality gap tolerance setting.

379 In contrast, RHA provides practical solutions for the optimal LCOCS at a significantly
 380 reduced computational cost by segmenting the entire optimization problem into several sub-
 381 problems. Specifically, as the foresight horizon of RHA increases, there is an improvement in
 382 solution accuracy and a proportional increase in computation time. For example, RHA ($u=2$)
 383 provides an optimal result of 392.27 $\$/t_{cs}$ which is better than the optimal result of RHA
 384 ($u=1$) (392.80 $\$/t_{cs}$). Extending the foresight horizon to 3 stages allows RHA ($u=3$) to obtain
 385 an optimal result of 392.20 $\$/t_{cs}$ with a computation time of 55.87 s, which is equal to the
 386 solution using RHA ($u=4$) and is better than the solution obtained by PSA in a reasonable
 387 time frame. The results demonstrate that RHA can provide high-quality solutions within an
 388 acceptable computation time, making it a practical and efficient approach for solving the MSEP
 389 model of RHSS.

390 4.3. Analysis of multi-stage expansion planning strategies

391 4.3.1. Investment strategies

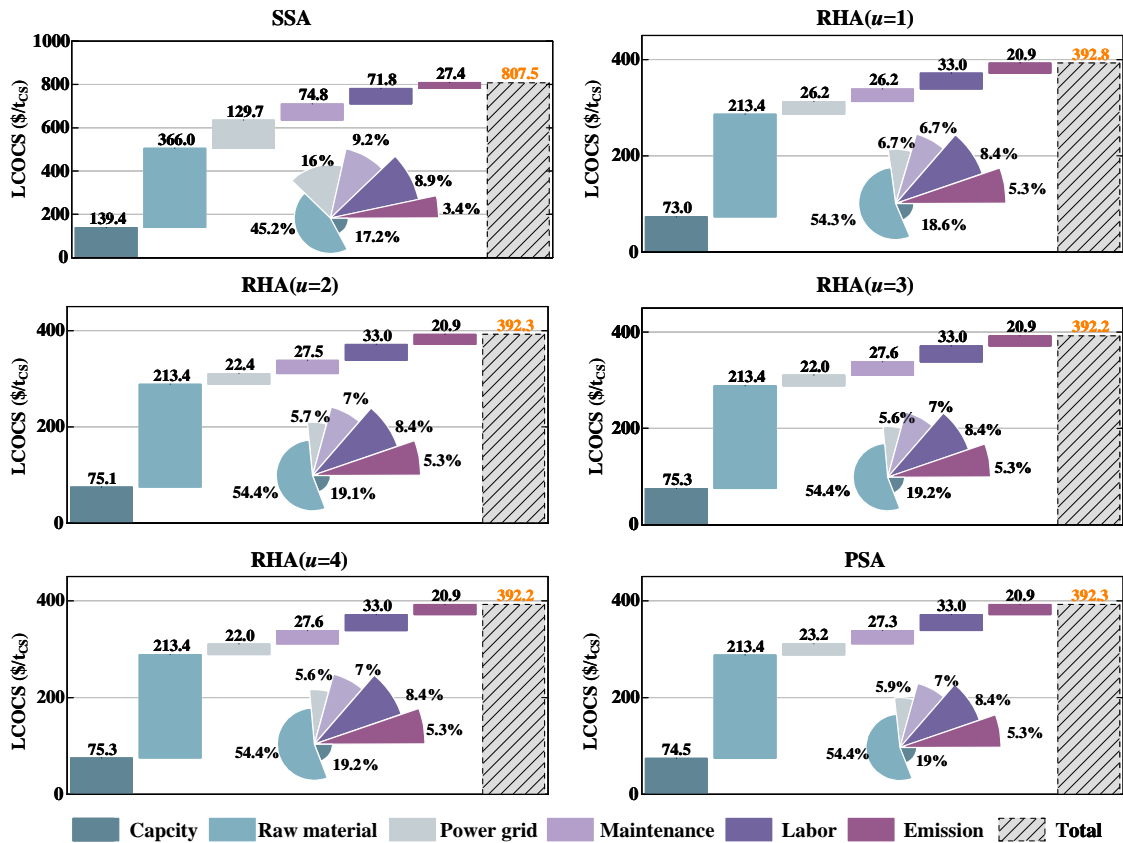


Fig. 7. Optimal LCOCS results using different approaches

392 Fig. 7 shows the breakdown of the LCOCS by different approaches, which include capacity
 393 investment costs, raw material costs, power grid costs, maintenance costs, labor costs, and
 394 emissions costs. Raw material costs account for the most significant portion of the LCOCS,

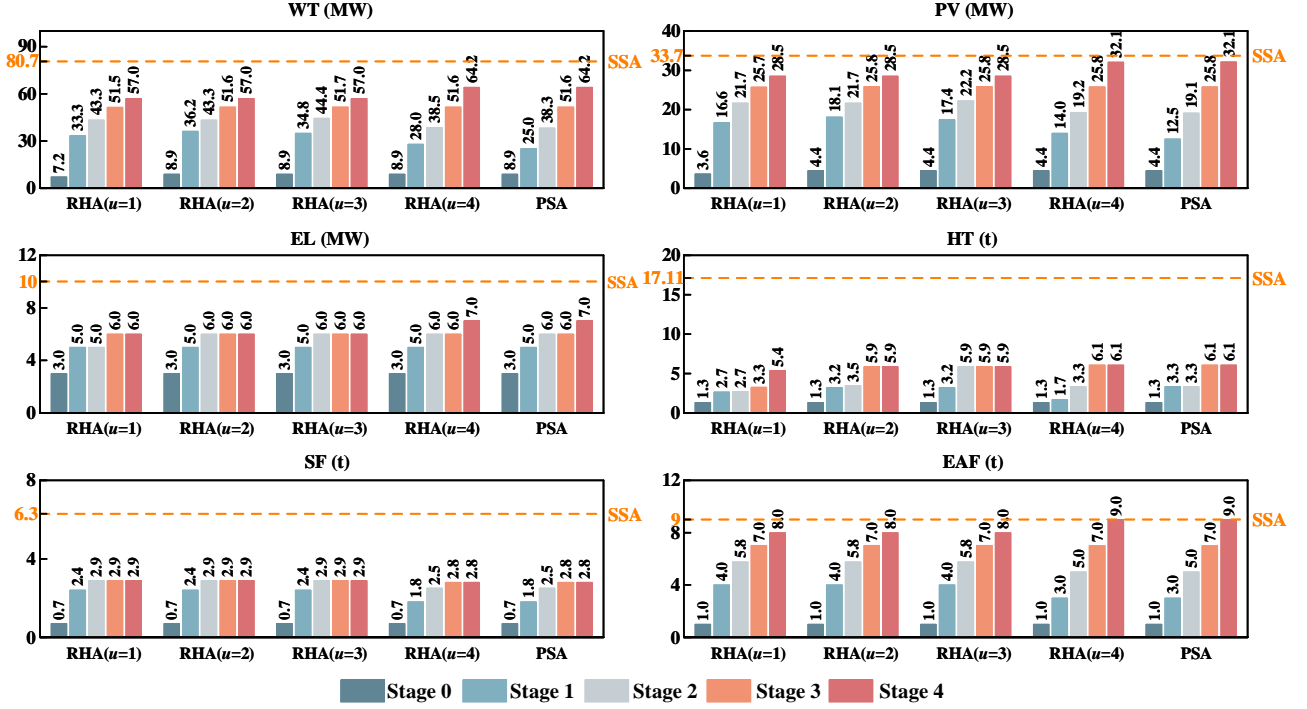


Fig. 8. Capacity investment strategies using different approaches

395 which are primarily influenced by the price of iron ore, lime, alloys, and carbon. In addition,
 396 as the steelmaking process evolves, the price of scrap steel has an increasing impact on raw
 397 material costs due to its growing share in production. Capacity costs are the second major
 398 component of the LCOCS. As technological advances lead to increased technical maturity over
 399 time, the associated capital costs decrease, thereby reducing capacity costs. Other associated
 400 costs, which are linked to capacity and raw material costs, respond to the dynamic changes in
 401 techno-economic parameters at each planning stage.

402 PSA and RHA facilitate a sequential investment strategy, allowing capacity expansion in
 403 stages, which helps minimize total costs. In contrast, SSA tends to result in the highest total
 404 cost of all components of the LCOCS. This approach focuses on a one-time, up-front investment
 405 in the initial planning stage, resulting in significant redundant initial investments and higher
 406 costs over time.

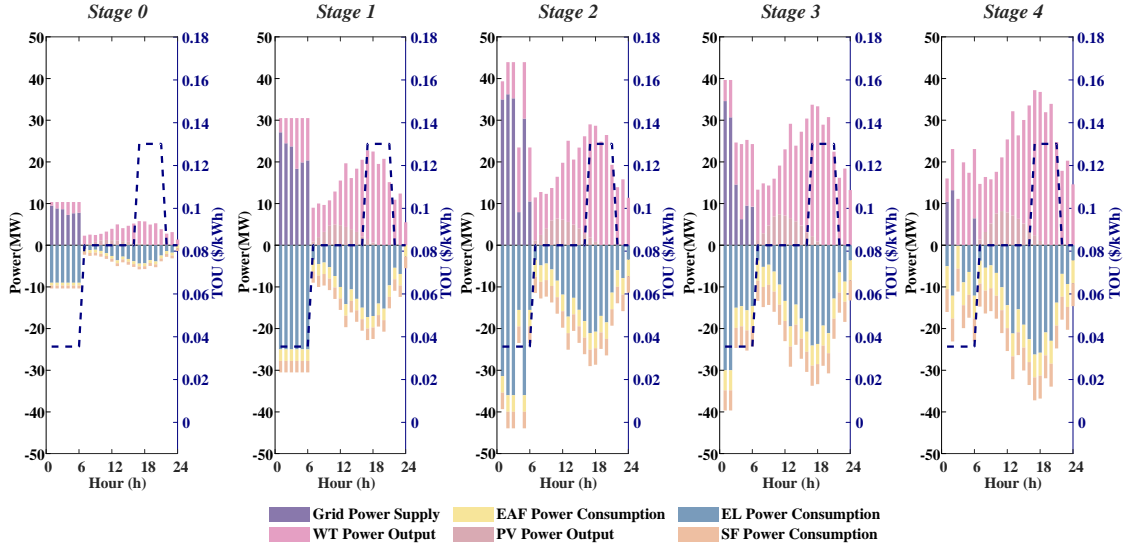
407 In the context of investment strategies, Fig. 8 shows the capacity configurations of WT,
 408 PV, EL, HT, SF, and EAF at each planning stage. The capacity configurations determined by
 409 SSA are shown with orange dotted lines, indicating that the capacities are fixed in the initial
 410 stage and remain unchanged throughout the planning horizon.

411 Over the planning horizon, the capacities of WT and PV are projected to increase by 7-8
 412 times, reflecting their roles in providing a stable supply of renewable energy and reducing CO₂
 413 emissions from the grid. This growth is in line with the expected increase in the use of wind
 414 and solar energy to support downstream processes in the steelmaking chain. The capacity of
 415 EL also increases over time to meet the growing demand for crude steel and the flexibility
 416 requirements of the system as the REP increases.

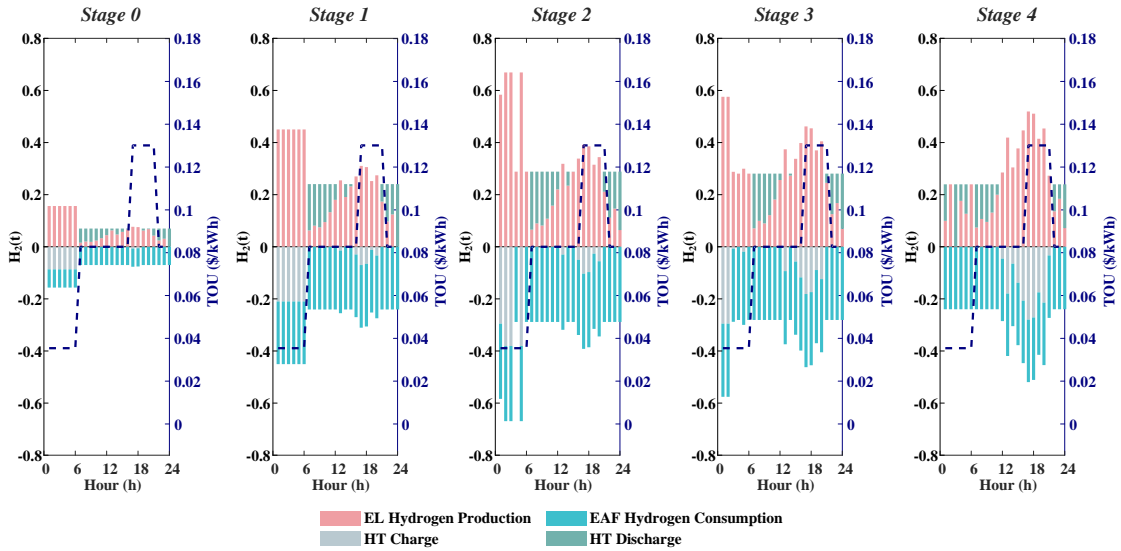
417 The capacity of EL will also increase over time to meet the growing demand for crude steel
 418 and to meet the flexibility needs of the system as renewable energy penetration increases. At
 419 the same time, the capacity of HT will be expanded to store excess hydrogen produced by
 420 EL during off-peak hours for use during peak demand periods, which underscores the growing
 421 importance of HT in balancing energy supply and demand within the system.

422 Similarly, the capacities of SF and EAF are being increased to meet the growing demand
 423 for crude steel. As the use of scrap steel in the steelmaking process increases, the capacity of
 424 the EAF will be gradually increased to optimize the recycling of scrap steel, further promote
 425 the energy efficiency and resource deployment of the steelmaking processes.

426 4.3.2. Operational strategies



(a) Electricity production and consumption



(b) Hydrogen production and consumption

Fig. 9. Optimal operation scheduling results at different planning stages using RHA ($u=4$)

427 Since RHA ($u=4$) achieves high-quality solutions within an acceptable computation time,
 428 we analyze the hourly operation of the system during a typical summer day using RHA ($u=4$),
 429 including patterns of electricity and hydrogen production and consumption.

430 As time-of-use (TOU) electricity prices fluctuate throughout the day, the operation strategy
 431 is dynamically adjusted. Production units are optimized to take advantage of lower electricity
 432 prices during off-peak hours, and to minimize consumption during peak hours, thereby reducing

433 the costs associated with purchasing grid electricity. In addition, HT plays a critical role by
 434 storing excess hydrogen produced by EL during off-peak periods for later use, increasing both
 435 operational flexibility of the system.

436 As the planning horizon progresses, the system’s operational strategy evolves in response
 437 to changes in the techno-economic parameters at each stage. In the initial stage, the system’s
 438 operation strategy is mainly based on the initial investment configuration, while in the following
 439 stages, the strategy is increasingly tailored to meet increasing load demands and incorporate a
 440 higher penetration of renewable energy sources, thus steering the generation structure towards
 441 greater sustainability and reducing CO₂ emissions from the grid.

442 Increased integration of RES introduces greater variability and intermittency into the sys-
 443 tem, necessitating increased reliance on storage technologies such as HT. These storage solutions
 444 are critical to maintaining a balance of energy supply and demand within the system, ensuring
 445 operational stability in the face of renewable variability.

446 *4.4. Analysis of environmental impacts*

447 The REP rate, as shown in Fig. 10, indicates that both RHA and PSA facilitate an in-
 448 cremental increase in REP, thereby reducing CO₂ emissions from the grid. Conversely, SSA
 449 maintains constant REP rates due to its fixed initial capacity configuration, which limits the
 450 ability of the system to promote a higher utilization of RES.

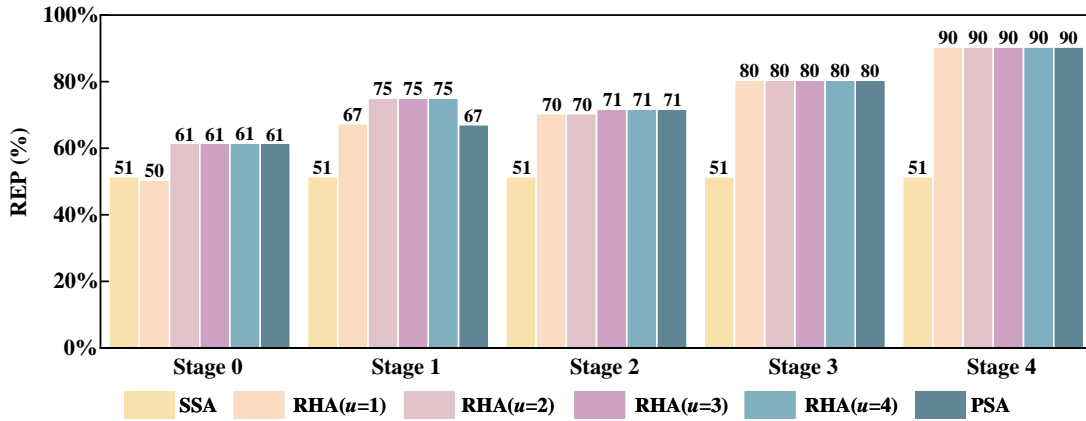


Fig. 10. REP rate over the planning horizon using RHA ($u=4$)

451 Fig. 11 shows the CO₂ intensity under different approaches. Implementation of the HDRI-
 452 EAF route, as in this study, results in significantly lower CO₂ intensities compared to the NG-
 453 DRI-EAF and BF-BOF routes (where the CO₂ intensity is 1000-1500 and 1500-2000 kg_{CO2}/t_{cs}
 454 respectively) [48]. Notably, the CO₂ intensity under SSA remains the highest throughout the
 455 planning stages, averaging 638.06 kg_{CO2}/t_{cs}. In contrast, the results for RHA are close to those
 456 for PSA, mainly due to the increasing REP rate and more extensive use of scrap steel in the
 457 steelmaking process.

458 These results indicate that RHA effectively supports long-term decarbonization goals in the
 459 steelmaking industry, demonstrating its potential to balance environmental performance with
 460 operational feasibility.

461 *4.5. Analysis of sensitivity and robustness*

462 As global targets for decarbonization and carbon neutrality evolve, policies will play a crucial
 463 role in shaping the demand for green steel production. Sensitivity and robustness analyses are
 464 conducted to assess the adaptability and effectiveness of our proposed approach considering

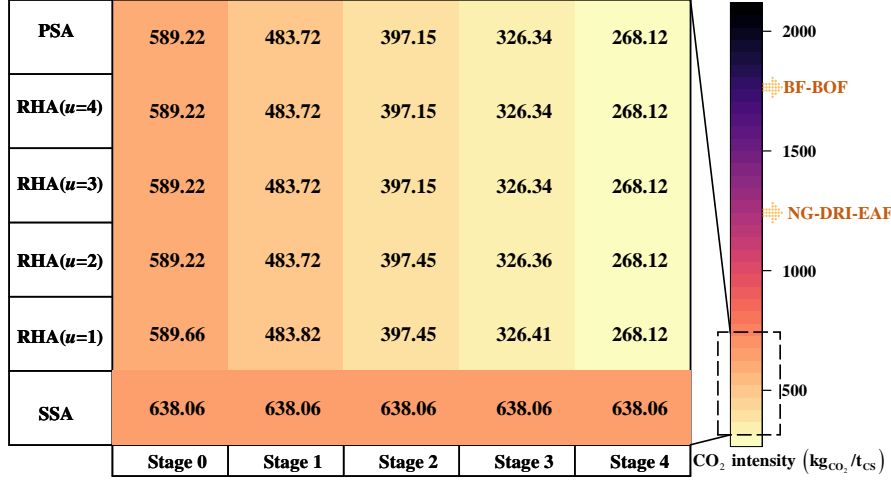


Fig. 11. CO₂ intensity over the planning horizon using RHA ($u=4$)

different steel demand scenarios and changes in techno-economic parameters to understand how different policy frameworks might affect system performance. We examine three different scenarios for crude steel demand growth to reflect potential future policy impacts (Fig. 12):

Scenario 1: Linear Growth

$L_0 = 1 \text{ t}_{\text{cs}}/\text{h}$, $\kappa = 2 \text{ t}_{\text{cs}}/\text{per stage}$.

Scenario 2: Slow Linear Growth followed by Fast Linear Growth

$L_0 = 1 \text{ t}_{\text{cs}}/\text{h}$, $i < 3$: $\kappa = 1 \text{ t}_{\text{cs}}/\text{h}$ per stage, $i \geq 3$: $\kappa = 3 \text{ t}_{\text{cs}}/\text{h}$ per stage.

Scenario 3: Fast Linear Growth followed by Slow Linear Growth

$L_0 = 1 \text{ t}_{\text{cs}}/\text{h}$, $i < 3$: $\kappa = 3 \text{ t}_{\text{cs}}/\text{h}$ per stage, $i \geq 3$: $\kappa = 1 \text{ t}_{\text{cs}}/\text{h}$ per stage.

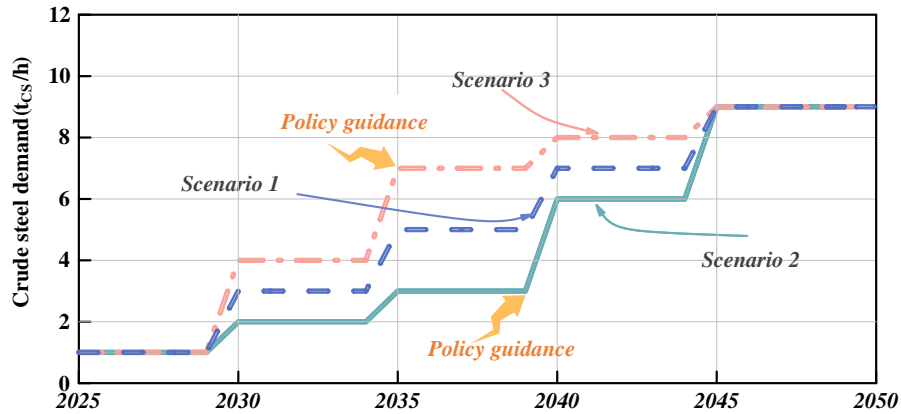


Fig. 12. Crude steel load growth trend under different scenarios

4.5.1. Sensitivity analysis

The sensitivity analysis visually and statistically compares the impact of different techno-economic parameters on the optimal LCOCS. In this section, QLab library [49] is used to perform a Sobol sensitivity analysis of the planning results obtained by RHA ($u=4$).

We evaluate the uncertainty of five key parameters: carbon tax, scrap steel price, iron ore price, labor cost, and discount rate in the sensitivity analysis, which are assumed to be uniformly distributed between predefined upper and lower bounds (Table 2). The results of the global sensitivity analysis are presented in the form of first-order Sobol indices and total-order Sobol indices, which are presented in Fig. 13.

483 The results indicate that the variability in the discount rate is a principal contributor to
 484 the overall uncertainty impacting the LCOCS, which suggests that the planning results are
 485 susceptible to changes in financing conditions. Additionally, the fluctuations in iron ore prices
 486 emerge as a significant determinant, followed by labor costs, scrap steel prices, and carbon tax.
 487 Given the dynamic nature of global economic and environmental policy, by understanding the
 488 multiple impacts of economics, environmental and technological factors on investment decisions,
 489 more scientifically rational planning strategies can be developed to support the transition to
 490 the sustainable development of ISI.

Table 2: Lower and upper bound of the input parameters for Sobol sensitivity analysis

Input parameters	Unit	Lower bound	Upper bound
c^{tax}	\$/tCO ₂	50	150
c^{scrap}	\$/t _{scrap}	300	400
c^{iron}	\$/t _{ore}	100	200
c^{labor}	\$/t _{cs}	50	100
r	%	0.04	0.10

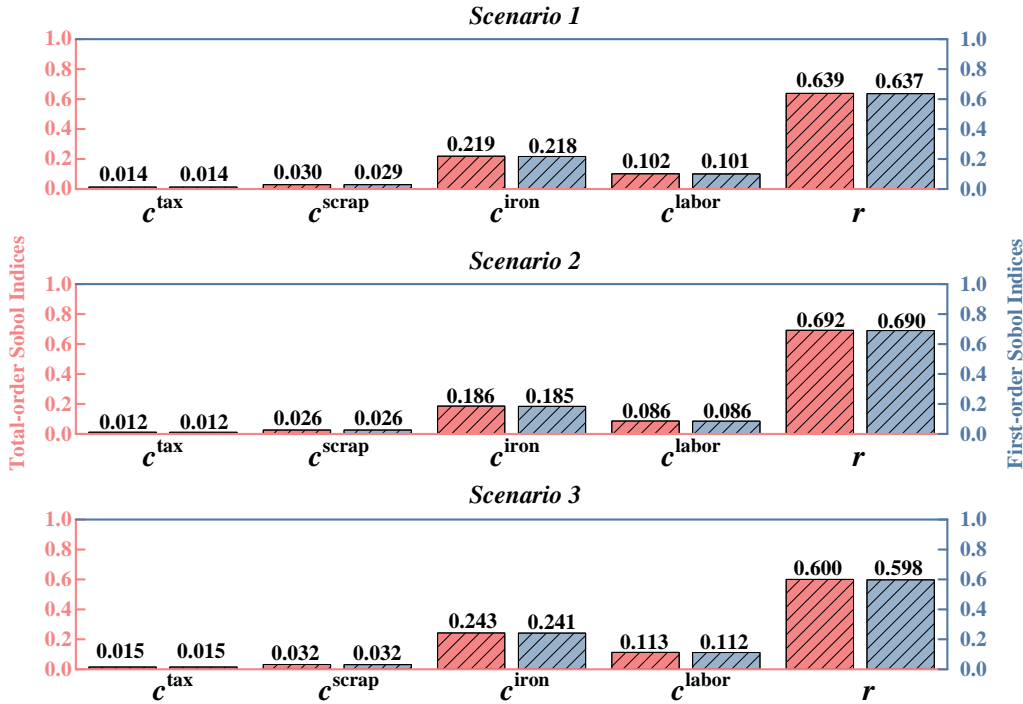


Fig. 13. Sensitivity analysis results of different input parameters using RHA ($u=4$)

491 4.5.2. Robustness analysis

492 Robustness analysis is performed to evaluate the adaptability of RHA under varying market
 493 demand and policy environments. The results of the optimal LCOCS and computation time
 494 using RHA ($u=4$) and PSA under different scenarios are shown in Table 3.

495 It's noteworthy that RHA ($u=4$) consistently achieves comparable or better cost efficiency
 496 than PSA in all scenarios. Meanwhile, the computation times of RHA ($u=4$) are significantly
 497 shorter than those of PSA in all three scenarios, which highlights the efficiency of RHA ($u=4$) in
 498 both economic and computational terms. As a result, RHA ($u=4$) emerges as a viable option for

499 real-world applications, particularly in solving large-scale optimization problems with complex
500 interactions over an extended planning horizon where convergence problems may occur in PSA.

501 The comparative results of REP rates and CO₂ intensities using RHA ($u=4$) and PSA
502 are presented in Table 4. Both approaches show consistent improvement in REP rates across
503 all three scenarios, demonstrating their effectiveness in promoting high-level usage of RES in
504 RHSS under different conditions. For the CO₂ intensity, both RHA ($u=4$) and PSA consistently
505 demonstrate a reduction across the stages, emphasizing their role in supporting the transition to
506 a more sustainable industrial processes by improving renewable energy integration and reducing
507 carbon emissions thereby decreasing the carbon footprint of steel production processes.

Table 3: Comparison of optimal LCOCS and computation time using RHA ($u=4$) and PSA under different scenarios

Scenario	Approach	LCOCS (\$/t _{CS})	Computation time (s)
Scenario 1	RHA ($u=4$)	392.20	327.90
	PSA	392.26	11434.97
Scenario 2	RHA ($u=4$)	387.48	377.17
	PSA	387.48	11672.50
Scenario 3	RHA ($u=4$)	395.45	392.08
	PSA	395.49	11635.72

Table 4: Combined Comparison of REP and CO₂ intensity using RHA ($u=4$) and PSA under different scenarios

Scenario	Approach	Stage				
		0	1	2	3	4
		REP (%) / CO ₂ intensity (kg _{CO₂} /t _{CS})				
Scenario 1	RHA ($u=4$)	61 / 589.22	75 / 483.49	71 / 397.14	80 / 326.40	90 / 268.12
	PSA	61 / 589.22	67 / 483.49	71 / 397.14	80 / 326.40	90 / 268.12
Scenario 2	RHA ($u=4$)	61 / 589.22	67 / 483.48	71 / 397.43	80 / 326.36	90 / 268.12
	PSA	61 / 588.63	67 / 483.53	71 / 397.14	80 / 326.33	90 / 268.12
Scenario 3	RHA ($u=4$)	61 / 589.22	69 / 483.72	71 / 397.15	80 / 326.34	90 / 268.12
	PSA	61 / 589.22	70 / 483.72	71 / 397.15	80 / 326.34	90 / 268.12

508 More detailed comparative results of SSA, RHA, and PSA are presented in Fig. A3 and
509 Fig. A4. Overall, the results demonstrate that RHA is a practical and robust approach for
510 solving the MSEP model of RHSS, providing high-quality solutions within reasonable compu-
511 tation time and effectively managing the incremental nature of decision-making in the MSEP
512 model.

513 5. Conclusion and perspectives

514 The decarbonization transformation of ISI is pivotal in the global quest for carbon neutrality.
515 The HDRI-EAF route holds significant potential to reduce CO₂ emissions in this sector. This
516 paper introduces a rolling-horizon approach to address the MSEP model of RHSS, covering
517 the planning horizon from 2025 to 2050. The novelty of this study lies in the development
518 of rational multi-stage investment strategies by considering the interactions between different
519 stages and the dynamic changes of techno-economic parameters.

520 The key findings demonstrate that, as the transition towards a low-carbon ISI takes shape,
521 the multi-stage expansion planning strategy is crucial for the economic and environmental

522 development of RHSS with a focus on long-term planning. RHA is proposed as a practical ap-
523 proach to address the complexity of the MSEP model, which can achieve high-quality solutions
524 with a reasonable computation time, overcoming the overinvestment limitations of SSA and re-
525 ducing the computational burdens of PSA. Notably, RHA is specifically designed to iteratively
526 incorporate the updated information, thereby increasing the robustness of the planning results.
527 In light of the ever-changing global economic and environmental policy landscape, it's imper-
528 ative to consider the multiple impacts of economic, environmental, and technological factors
529 on investment decisions. RHA exemplifies this by providing robust and adaptive multi-stage
530 expansion planning strategies that specifically support the transition toward sustainable and
531 low-carbon steel production.

532 Future research will focus on exploring the cumulative impact of parameter uncertainty on
533 planning results, addressing the inherent myopic nature of the current RHA model, which will
534 further refine our understanding and implementation of robust planning strategies in the face
535 of uncertainty. Moreover, the potential integration of different renewable energy sources will
536 be explored to further enhance the sustainability of RHSS and support the global transition to
537 a low-carbon steelmaking process.

538 **Credit author contribution statement**

539 **Kangling Sheng:** Methodology, Software, Writing - original draft. **Xiaojun Wang:**
540 Conceptualization,, Writing - review& editing. **Fangyuan Si:** Conceptualization, Writing - re-
541 view& editing. **Yue Zhou:** Conceptualization, Writing - review& editing. **Zhao Liu:** Writing
542 - review& editing. **Haochen Hua:** Writing - review& editing. **Xihao Wang:** Supervision.
543 **Yuge Duan:** Supervision.

544 **Declaration of competing interest**

545 The authors declare that they have no known competing financial interests or personal
546 relationships that could have appeared to influence the work reported in this paper.

547 **Data availability**

548 Data will be made available on request.

549 **Acknowledgment**

550 This work was supported by the National Nature Science Foundation of China [Grant
551 Number: 52207112] and Beijing Jiaotong University Talent Fund Project [Grant Number: 2024
552 RC001].

553 References

- 554 [1] Aljoša Slameršak, Giorgos Kallis, and Daniel W. O’Neill. Energy requirements and carbon emissions for a low-carbon energy transition. *Nature Communications*, 13(1):6932, November 2022. ISSN 2041-1723. doi: 10.1038/s41467-022-33976-5.
- 555
- 556
- 557 [2] Net Zero by 2050 – Analysis. <https://www.iea.org/reports/net-zero-by-2050>, May 2021.
- 558 [3] Iron and Steel Technology Roadmap – Analysis. <https://www.iea.org/reports/iron-and-steel-technology-roadmap>, October 2020.
- 559
- 560 [4] Steel Climate Impact - An International Benchmarking of Energy and CO2 Intensities. <https://www.globalefficiencyintel.com/steel-climate-impact-international-benchmarking-energy-co2-intensities>.
- 561
- 562
- 563 [5] Zhuo Kang, Qingliang Liao, Zheng Zhang, and Yue Zhang. Carbon neutrality orientates the reform of the steel industry. *Nature Materials*, 21(10):1094–1098, October 2022. ISSN 1476-4660. doi: 10.1038/s41563-022-01370-7.
- 564
- 565
- 566 [6] World Steel in Figures 2023 - worldsteel.org. <https://worldsteel.org/data/world-steel-in-figures-2023/>.
- 567
- 568 [7] Silvia Madeddu, Falko Ueckerdt, Michaja Pehl, Juergen Peterseim, Michael Lord, Karthik Ajith Kumar, Christoph Krüger, and Gunnar Luderer. The CO2 reduction potential for the European industry via direct electrification of heat supply (power-to-heat). *Environmental Research Letters*, 15(12):124004, November 2020. ISSN 1748-9326. doi: 10.1088/1748-9326/abbd02.
- 569
- 570
- 571
- 572
- 573 [8] Annika Boldrini, Derck Koolen, Wina Crijns-Graus, Ernst Worrell, and Machteld van den Broek. Flexibility options in a decarbonising iron and steel industry. *Renewable and Sustainable Energy Reviews*, 189:113988, January 2024. ISSN 1364-0321. doi: 10.1016/j.rser.2023.113988.
- 574
- 575
- 576
- 577 [9] Lingzhi Yang, Hang Hu, Mengxian Wang, Feng Chen, Shuai Wang, Yufeng Guo, Sheng Yang, and Tao Jiang. Comparative life cycle assessment and techno-economic analysis of electric arc furnace steelmaking processes integrated with solar energy system. *Journal of Cleaner Production*, 425:138868, November 2023. ISSN 0959-6526. doi: 10.1016/j.jclepro.2023.138868.
- 578
- 579
- 580
- 581
- 582 [10] Hassan Elsheikh and Valerie Eveloy. Assessment of variable solar- and grid electricity-driven power-to-hydrogen integration with direct iron ore reduction for low-carbon steel making. *Fuel*, 324:124758, September 2022. ISSN 0016-2361. doi: 10.1016/j.fuel.2022.124758.
- 583
- 584
- 585
- 586 [11] Joint Research Centre (European Commission), Derck Koolen, and Derck Vidovic. *Greenhouse Gas Intensities of the EU Steel Industry and Its Trading Partners*. Publications Office of the European Union, 2022. ISBN 978-92-76-53417-4.
- 587
- 588
- 589 [12] Lingzhi Yang, Hang Hu, Mengxian Wang, Feng Chen, Shuai Wang, Yufeng Guo, Sheng Yang, and Tao Jiang. Comparative life cycle assessment and techno-economic analysis of electric arc furnace steelmaking processes integrated with solar energy system. *Journal of Cleaner Production*, 425:138868, November 2023. ISSN 0959-6526. doi: 10.1016/j.jclepro.2023.138868.
- 590
- 591
- 592
- 593
- 594 [13] IEA – International Energy Agency. <https://www.iea.org>.
- 595 [14] Govinda R. Timilsina. Are renewable energy technologies cost competitive for electricity generation? *Renewable Energy*, 180:658–672, December 2021. ISSN 0960-1481. doi: 10.1016/j.renene.2021.08.088.
- 596
- 597

- 598 [15] G. Kakoulaki, I. Kougiyas, N. Taylor, F. Dolci, J. Moya, and A. Jäger-Waldau. Green hydro-
599 gen in Europe – A regional assessment: Substituting existing production with electrolysis
600 powered by renewables. *Energy Conversion and Management*, 228:113649, January 2021.
601 ISSN 0196-8904. doi: 10.1016/j.enconman.2020.113649.
- 602 [16] Zhiyuan Fan and S. Julio Friedmann. Low-carbon production of iron and steel: Technology
603 options, economic assessment, and policy. *Joule*, 5(4):829–862, April 2021. ISSN 2542-
604 4351. doi: 10.1016/j.joule.2021.02.018.
- 605 [17] Ruochong Xu, Dan Tong, Steven J. Davis, Xinying Qin, Jing Cheng, Qinren Shi, Yang
606 Liu, Cuihong Chen, Liu Yan, Xizhe Yan, Huaxuan Wang, Dongsheng Zheng, Kebin He,
607 and Qiang Zhang. Plant-by-plant decarbonization strategies for the global steel industry.
608 *Nature Climate Change*, 13(10):1067–1074, October 2023. ISSN 1758-6798. doi: 10.1038/
609 s41558-023-01808-z.
- 610 [18] H2future - VERBUND. [https://www.verbund.com/en-at/about-verbund/news-
611 press/press-releases/2017/02/07/hydrogen](https://www.verbund.com/en-at/about-verbund/news-press/press-releases/2017/02/07/hydrogen).
- 612 [19] Our program SALCOS®. <https://salcos.salzgitter-ag.com/en/salcos.html>.
- 613 [20] POSCO. Carbon Neutral Strategy - Carbon Neutrality - POSCO.
614 <https://www.posco.co.kr/>.
- 615 [21] China’s first 1 million ton hydrogen-based shaft furnace began production at Baosteel
616 Zhanjiang. <https://chinahydrogen.substack.com/p/chinas-first-1-million-ton-hydrogen>, .
- 617 [22] R. R. Wang, Y. Q. Zhao, A. Babich, D. Senk, and X. Y. Fan. Hydrogen direct reduction (H-
618 DR) in steel industry—An overview of challenges and opportunities. *Journal of Cleaner
619 Production*, 329:129797, December 2021. ISSN 0959-6526. doi: 10.1016/j.jclepro.2021.
620 129797.
- 621 [23] MIDREX H₂. <https://www.midrex.com/technology/midrex-process/midrex-h2/>.
- 622 [24] Yongli Wang, Yudong Wang, Yujing Huang, Fang Li, Ming Zeng, Jiapu Li, Xiaohai Wang,
623 and Fuwei Zhang. Planning and operation method of the regional integrated energy system
624 considering economy and environment. *Energy*, 171:731–750, March 2019. ISSN 0360-5442.
625 doi: 10.1016/j.energy.2019.01.036.
- 626 [25] Miguel Asensio and Javier Contreras. Stochastic Unit Commitment in Isolated Systems
627 With Renewable Penetration Under CVaR Assessment. *IEEE Transactions on Smart Grid*,
628 7(3):1356–1367, May 2016. ISSN 1949-3061. doi: 10.1109/TSG.2015.2469134.
- 629 [26] Tao Ding, Shiyu Liu, Wei Yuan, Zhaohong Bie, and Bo Zeng. A Two-Stage Robust
630 Reactive Power Optimization Considering Uncertain Wind Power Integration in Active
631 Distribution Networks. *IEEE Transactions on Sustainable Energy*, 7(1):301–311, January
632 2016. ISSN 1949-3037. doi: 10.1109/TSTE.2015.2494587.
- 633 [27] Alla Toktarova, Lisa Göransson, and Filip Johnsson. Design of Clean Steel Production
634 with Hydrogen: Impact of Electricity System Composition. *Energies*, 14(24):8349, January
635 2021. ISSN 1996-1073. doi: 10.3390/en14248349.
- 636 [28] Francesco Superchi, Alessandro Mati, Carlo Carcasci, and Alessandro Bianchini. Techno-
637 economic analysis of wind-powered green hydrogen production to facilitate the decar-
638 bonization of hard-to-abate sectors: A case study on steelmaking. *Applied Energy*, 342:
639 121198, July 2023. ISSN 0306-2619. doi: 10.1016/j.apenergy.2023.121198.
- 640 [29] Valentin Vogl, Max Åhman, and Lars J. Nilsson. Assessment of hydrogen direct reduction
641 for fossil-free steelmaking. *Journal of Cleaner Production*, 203:736–745, December 2018.
642 ISSN 0959-6526. doi: 10.1016/j.jclepro.2018.08.279.

- 643 [30] Abhinav Bhaskar, Rockey Abhishek, Mohsen Assadi, and Homam Nikpey Somehesaraei.
644 Decarbonizing primary steel production : Techno-economic assessment of a hydrogen based
645 green steel production plant in Norway. *Journal of Cleaner Production*, 350:131339, May
646 2022. ISSN 0959-6526. doi: 10.1016/j.jclepro.2022.131339.
- 647 [31] Hassan Elsheikh and Valerie Eveloy. Renewable hydrogen based direct iron ore reduction
648 and steel making with grid assistance. *Energy Conversion and Management*, 297:117544,
649 December 2023. ISSN 0196-8904. doi: 10.1016/j.enconman.2023.117544.
- 650 [32] Andrew J. Pimm, Tim T. Cockerill, and William F. Gale. Energy system requirements
651 of fossil-free steelmaking using hydrogen direct reduction. *Journal of Cleaner Production*,
652 312:127665, 2021.
- 653 [33] L. Gacitua, P. Gallegos, R. Henriquez-Auba, Á. Lorca, M. Negrete-Pincetic, D. Olivares,
654 A. Valenzuela, and G. Wenzel. A comprehensive review on expansion planning: Models and
655 tools for energy policy analysis. *Renewable and Sustainable Energy Reviews*, 98:346–360,
656 December 2018. ISSN 1364-0321. doi: 10.1016/j.rser.2018.08.043.
- 657 [34] Ang Xuan, Xinwei Shen, Qinglai Guo, and Hongbin Sun. A conditional value-at-risk based
658 planning model for integrated energy system with energy storage and renewables. *Applied*
659 *Energy*, 294:116971, July 2021. ISSN 0306-2619. doi: 10.1016/j.apenergy.2021.116971.
- 660 [35] Guangsheng Pan, Wei Gu, Haifeng Qiu, Yuping Lu, Suyang Zhou, and Zhi Wu. Bi-
661 level mixed-integer planning for electricity-hydrogen integrated energy system considering
662 leveled cost of hydrogen. *Applied Energy*, 270:115176, July 2020. ISSN 0306-2619. doi:
663 10.1016/j.apenergy.2020.115176.
- 664 [36] Amr A. Hamad, Mohammed Elsayed Nassar, Ehab F. El-Saadany, and M. M. A. Salama.
665 Optimal Configuration of Isolated Hybrid AC/DC Microgrids. *IEEE Transactions on*
666 *Smart Grid*, 10(3):2789–2798, May 2019. ISSN 1949-3061. doi: 10.1109/TSG.2018.
667 2810310.
- 668 [37] Ahmed M. Elberry, Jagruti Thakur, and Jason Veysey. Seasonal hydrogen storage for
669 sustainable renewable energy integration in the electricity sector: A case study of Finland.
670 *Journal of Energy Storage*, 44:103474, December 2021. ISSN 2352-152X. doi: 10.1016/j.
671 est.2021.103474.
- 672 [38] David U. Ziegler, Carlos Mateo, Tomás Gómez San Román, and Giuseppe Pretticco. Mul-
673 tistage distribution expansion planning leveraging load flexibility. *Electric Power Systems*
674 *Research*, 228:110094, March 2024. ISSN 0378-7796. doi: 10.1016/j.eprsr.2023.110094.
- 675 [39] Zhinong Wei, Li Yang, Sheng Chen, Zhoujun Ma, Haixiang Zang, and Youdie Fei. A
676 multi-stage planning model for transitioning to low-carbon integrated electric power and
677 natural gas systems. *Energy*, 254:124361, September 2022. ISSN 0360-5442. doi: 10.1016/
678 j.energy.2022.124361.
- 679 [40] Markus Bohlayer, Adrian Bürger, Markus Fleschutz, Marco Braun, and Gregor Zöttl.
680 Multi-period investment pathways - Modeling approaches to design distributed energy
681 systems under uncertainty. *Applied Energy*, 285:116368, March 2021. ISSN 0306-2619.
682 doi: 10.1016/j.apenergy.2020.116368.
- 683 [41] Yang Lei, Dan Wang, Hongjie Jia, Jiayi Li, Jingcheng Chen, Jingru Li, and Zhihong Yang.
684 Multi-stage stochastic planning of regional integrated energy system based on scenario tree
685 path optimization under long-term multiple uncertainties. *Applied Energy*, 300:117224,
686 October 2021. ISSN 0306-2619. doi: 10.1016/j.apenergy.2021.117224.
- 687 [42] Ilkka Keppo and Manfred Strubegger. Short term decisions for long term problems—The
688 effect of foresight on model based energy systems analysis. *Energy*, 35(5):2033–2042, 2010.

- 689 [43] Siyu Feng, Hongtao Ren, and Wenji Zhou. A review of uncertain factors and analytic
690 methods in long-term energy system optimization models. *Global Energy Interconnection*,
691 6(4):450–466, August 2023. ISSN 2096-5117. doi: 10.1016/j.gloi.2023.08.006.
- 692 [44] Lukas Glomb, Frauke Liers, and Florian Rösel. A rolling-horizon approach for multi-period
693 optimization. *European Journal of Operational Research*, 300(1):189–206, July 2022. ISSN
694 0377-2217. doi: 10.1016/j.ejor.2021.07.043.
- 695 [45] T. Ross Archibald. The Return to Straight-Line Depreciation: An Analysis of a Change in
696 Accounting Method. *Journal of Accounting Research*, 5:164–180, 1967. ISSN 0021-8456.
697 doi: 10.2307/2489918.
- 698 [46] Bryan S. Palmintier and Mort D. Webster. Heterogeneous Unit Clustering for Efficient
699 Operational Flexibility Modeling. *IEEE Transactions on Power Systems*, 29(3):1089–1098,
700 May 2014. ISSN 1558-0679. doi: 10.1109/TPWRS.2013.2293127.
- 701 [47] Gurobi Optimizer Release Notes v10.0.1 - Gurobi Optimization.
702 <https://www.gurobi.com/downloads/gurobi-optimizer-release-notes-v10-0-1/>.
- 703 [48] Yifan Chang, Fang Wan, Xilong Yao, Jianxin Wang, Yunfei Han, and Hui Li. Influence
704 of hydrogen production on the CO2 emissions reduction of hydrogen metallurgy transfor-
705 mation in iron and steel industry. *Energy Reports*, 9:3057–3071, December 2023. ISSN
706 2352-4847. doi: 10.1016/j.egyr.2023.01.083.
- 707 [49] Getting UQLab. <https://www.uqlab.com/download>.
- 708 [50] Abhinav Bhaskar, Mohsen Assadi, and Homam Nikpey Somehsaraei. Decarbonization
709 of the Iron and Steel Industry with Direct Reduction of Iron Ore with Green Hydrogen.
710 *Energies*, 13(3):758, January 2020. ISSN 1996-1073. doi: 10.3390/en13030758.
- 711 [51] Andries Krüger, Joakim Andersson, Stefan Grönkvist, and Ann Cornell. Integration of
712 water electrolysis for fossil-free steel production. *International Journal of Hydrogen Energy*,
713 45(55):29966–29977, November 2020. ISSN 0360-3199. doi: 10.1016/j.ijhydene.2020.08.
714 116.
- 715 [52] Gabriel Lopez, Javier Farfan, and Christian Breyer. Trends in the global steel industry:
716 Evolutionary projections and defossilisation pathways through power-to-steel. *Journal of*
717 *Cleaner Production*, 375:134182, November 2022. ISSN 0959-6526. doi: 10.1016/j.jclepro.
718 2022.134182.
- 719 [53] Coking Coal Price: Charts, Forecasts & News - FocusEconomics. [https://www.focus-](https://www.focus-economics.com/commodities/energy/coking-coal/)
720 [economics.com/commodities/energy/coking-coal/](https://www.focus-economics.com/commodities/energy/coking-coal/).
- 721 [54] Herbert Pfeifer and Marcus Kirschen. Thermodynamic analysis of EAF energy efficiency
722 and comparison with a statistical model of electric energy demand. In *7th European Electric*
723 *Steelmaking Conference*, volume 26, page 1. Citeseer, 2002.
- 724 [55] China: Power sector carbon intensity 2022. [https://www.statista.com/statistics/1300419/power-](https://www.statista.com/statistics/1300419/power-generation-emission-intensity-china/)
725 [generation-emission-intensity-china/](https://www.statista.com/statistics/1300419/power-generation-emission-intensity-china/), .

Appendix A

Table A1: Assumptions of CAPEX and OPEX from 2025 to 2050 in this study

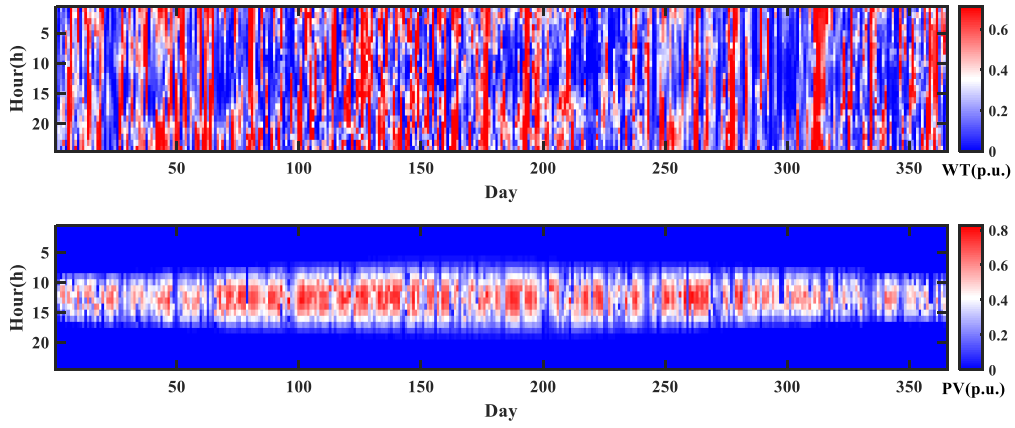
Equipment	Unit	CAPEX					OPEX(%)	Technical Life (a)	Ref
		2025	2030	2035	2040	2045			
WT	\$/kW	1500	1400	1300	1200	1100	3	30	[28]
PV	\$/kW	1000	900	800	700	600	3	30	[28]
EL	\$/kW	900	800	700	600	500	5	25	[50]
HT	\$/kg _{H₂}	500					5	30	[50]
SF	\$/t _{DRI} · a	250					8	40	[51]
EAF	\$/t _{cs} · a	230					8	40	[51]

*Each EL module has a capacity of 1 MWh.

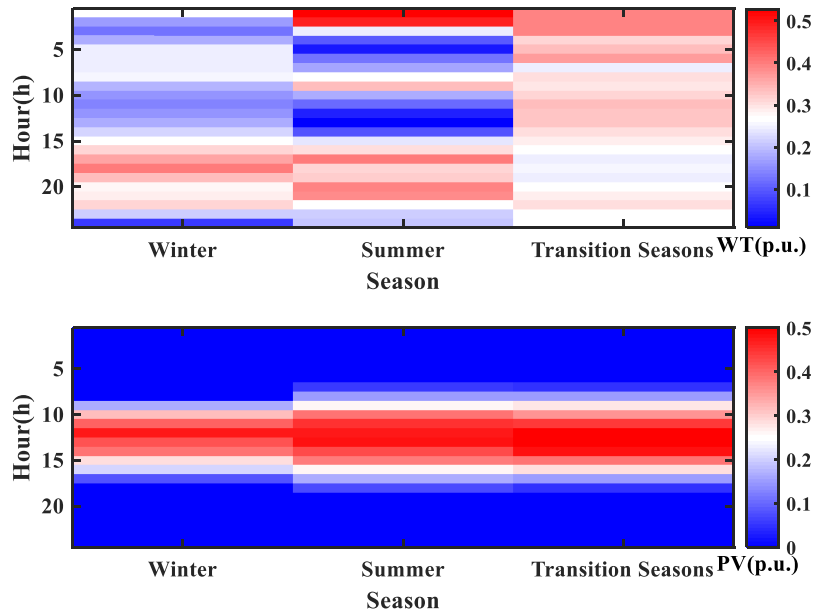
Table A3: Assumptions of associated parameters from 2025 to 2050 in this study

Associated parameters	Unit	2025	2030	2035	2040	2045	Ref
Renewable energy penetration	%	50	60	70	80	90	-
CO ₂ intensity	t _{CO₂} /t _{cs}	700	600	500	400	300	[10]
EL efficiency	kWh/kg _{H₂}	60	55	50	45	40	[50]
Crude steel demand	t _{cs} /h	1	2	4	6	8	-
Scrap steel rate	t _{scrap} /t _{cs}	0.3	0.4	0.5	0.6	0.7	[52]
Scrap steel cost	\$/t _{scrap}	328					[9]
Labor cost	\$/t _{cs}	60					[53]
EAF alloys demand	kg/t _{cs}	11					[9]
EAF alloys cost	\$/t	1500					[9]
EAF lime demand	kg/t _{cs}	50					[9]
EAF lime cost	\$/t	110					[9]
EAF carbon demand	kg/t _{cs}	20					[54]
EAF carbon cost	\$/t	180					[53]
Iron ore demand	t _{iron} /t _{cs}	1.5					[52]
Iron ore cost	\$/t _{iron}	122					[50]
Crude steel production EF	kg _{CO₂} /t _{cs}	130					[50]
Iron ore production EF	kg _{CO₂} /t _{cs}	167					[50]
Grid-average EF	kg _{CO₂} /kWh	0.57					[55]
Carbon tax	\$/t _{CO₂}	60					[54]

*Other associated parameters are from Ref [50].



(a) Normalized WT/PV generation during typical metric year



(b) Normalized WT/PV generation during typical seasonal days

Fig. A1. Normalized WT/PV generation

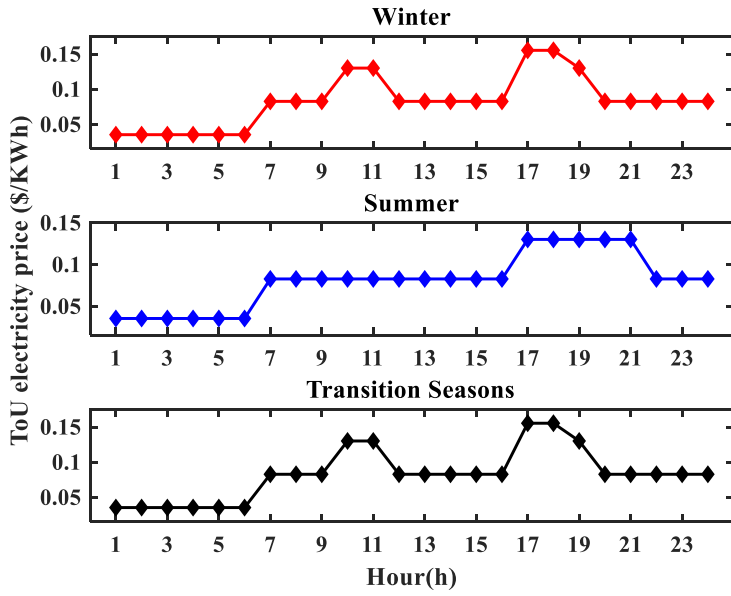


Fig. A2. TOU electricity prices for a typical day

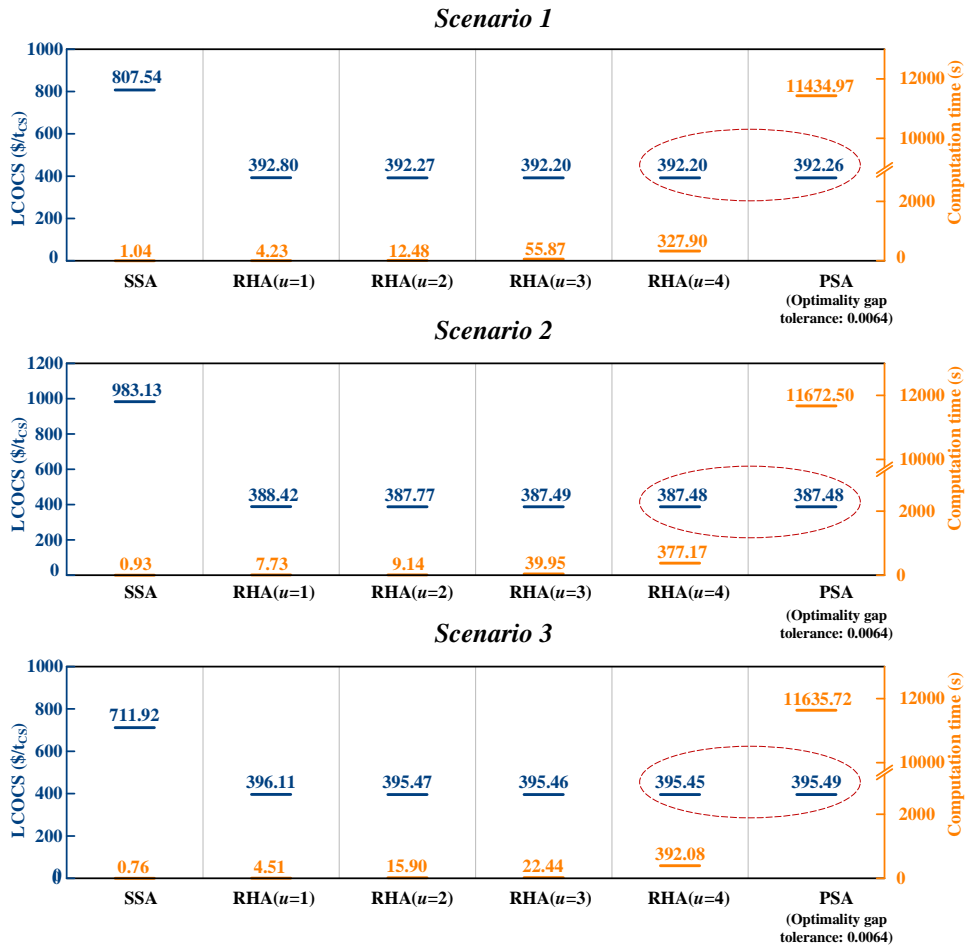
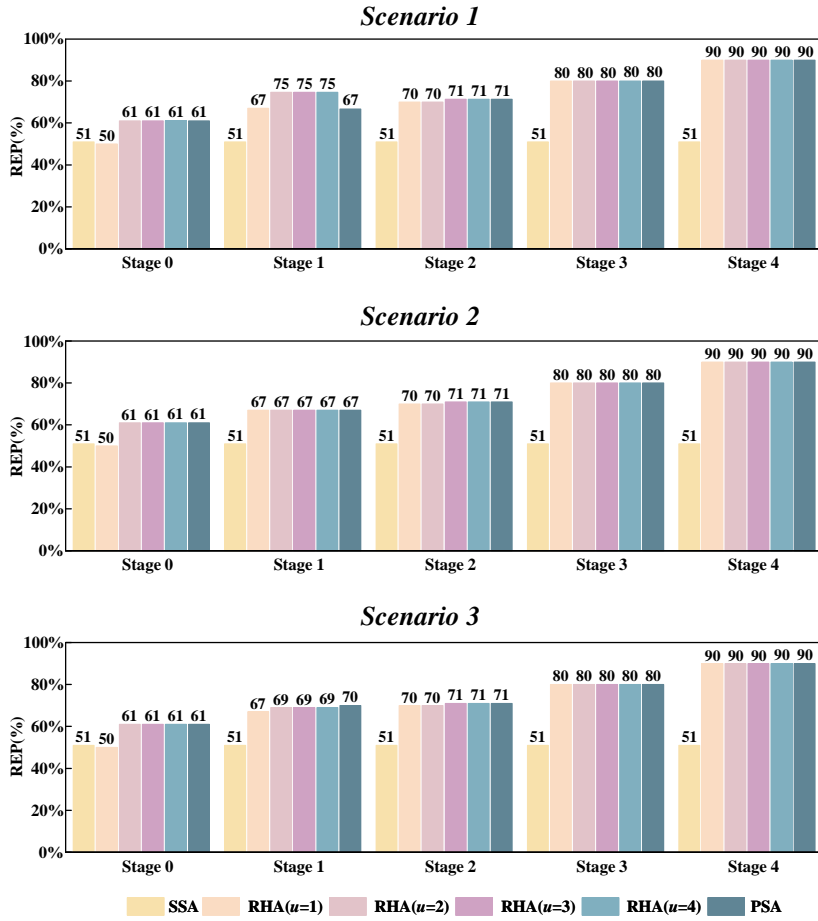
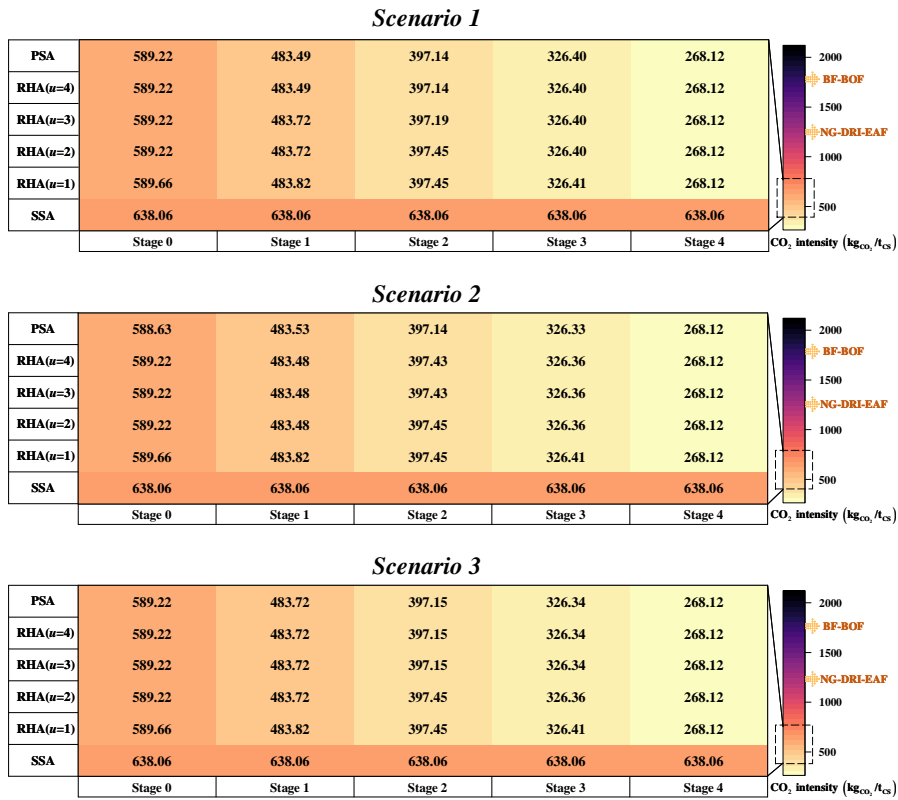


Fig. A3. Comparison of optimal LCOCS and computation time under different scenarios using different approaches



(a) REP rate



(b) CO₂ intensity

Fig. A4. Comparison of REP rate and CO₂ intensity under different scenarios using different approaches